Article

Cell Reports

Muscarinic Acetylcholine Receptors *Chrm1* and *Chrm3* Are Essential for REM Sleep

Graphical Abstract

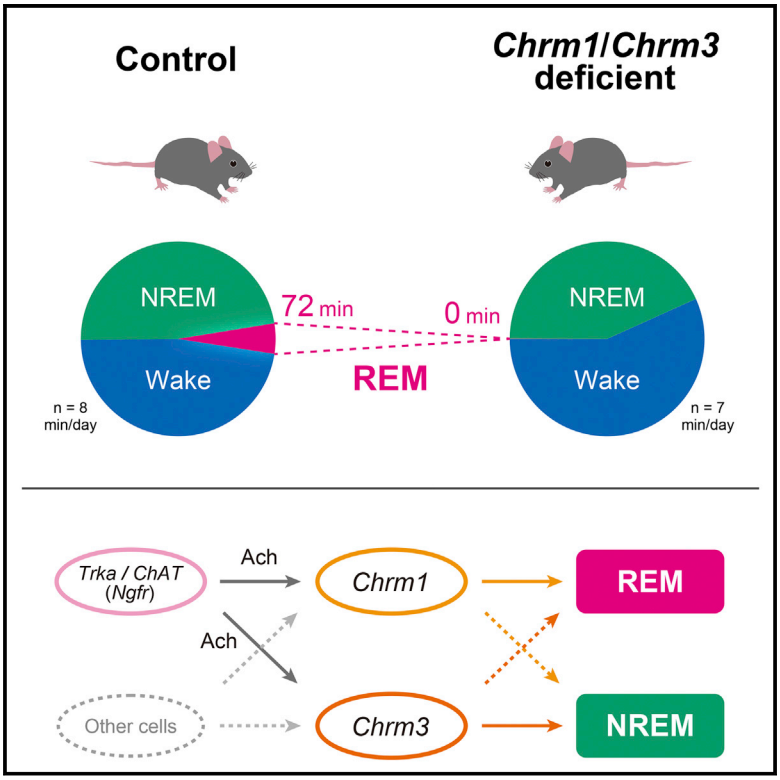

Authors

Yasutaka Niwa, Genki N. Kanda, Rikuhiro G. Yamada, ..., Hiroshi Kiyonari, Kenta Sumiyama, Hiroki R. Ueda

Correspondence

uedah-tky@umin.ac.jp

In Brief

The acetylcholine pathway has been proposed to be important for wakefulness and REM sleep, but genetic evidence has been missing. Using a knockout of acetylcholine receptor genes, Niwa et al. show that *Chrm1* and *Chrm3* double knockout chronically diminishes REM sleep to an undetectable level and causes a severe short-sleep phenotype.

Highlights

- Inhibition of *TrkA*+ cholinergic neurons causes a severe short-sleep phenotype in mice
- Knockout of the muscarinic acetylcholine receptors *Chrm1* and *Chrm3* reduces NREM sleep
- Knockout of *Chrm1* and *Chrm3* reduces and fragments REM sleep, respectively
- *Chrm1* and *Chrm3* are essential for REM sleep

Niwa et al., 2018, Cell Reports *24*, 2231–2247
August 28, 2018
https://doi.org/10.1016/j.celrep.2018.07.082

CellPress

Cell Reports
Article

Muscarinic Acetylcholine Receptors *Chrm1* and *Chrm3* Are Essential for REM Sleep

Yasutaka Niwa,[1,2,14] Genki N. Kanda,[1,3,4,14] Rikuhiro G. Yamada,[1,14] Shoi Shi,[1,5,6] Genshiro A. Sunagawa,[1,4] Maki Ukai-Tadenuma,[1,6] Hiroshi Fujishima,[1] Naomi Matsumoto,[7] Koh-hei Masumoto,[8,9,10] Mamoru Nagano,[8] Takeya Kasukawa,[11] James Galloway,[12] Dimitri Perrin,[1,12] Yasufumi Shigeyoshi,[8] Hideki Ukai,[1,6] Hiroshi Kiyonari,[13] Kenta Sumiyama,[7] and Hiroki R. Ueda[1,5,6,15,*]

[1]Laboratory for Synthetic Biology, RIKEN Center for Biosystems Dynamics Research, 1-3 Yamadaoka, Suita, Osaka 565-0871, Japan
[2]International Institute for Integrative Sleep Medicine, University of Tsukuba, 1-1-1 Tennodai, Tsukuba, Ibaraki 305-8575, Japan
[3]Graduate School of Frontier Biosciences, Osaka University, 1-3 Yamadaoka, Suita, Osaka 565-0871, Japan
[4]Laboratory for Retinal Regeneration, RIKEN Center for Biosystems Dynamics Research, 2-2-3 Minatojima Minamimachi, Chuo-ku, Kobe, Hyogo 650-0047, Japan
[5]Department of Systems Pharmacology, Graduate School of Medicine, The University of Tokyo, 7-3-1 Hongo, Bunkyo-ku, Tokyo 113-0033, Japan
[6]International Research Center for Neurointelligence (WPI-IRCN), The University of Tokyo Institutes for Advanced Study (UTIAS), The University of Tokyo, 7-3-1 Hongo, Bunkyo-ku, Tokyo 113-0033, Japan
[7]Laboratory for Mouse Genetic Engineering, RIKEN Center for Biosystems Dynamics Research, 1-3 Yamadaoka, Suita, Osaka 565-0871, Japan
[8]Department of Anatomy and Neurobiology, Kindai University Faculty of Medicine, 377-2 Ohno-Higashi, Osakasayama City, Osaka 589-8511, Japan
[9]Center for Medical Science, International University of Health and Welfare, 2600-1 Kitakanemaru, Ohtawara, Tochigi 324-8501, Japan
[10]Division of Neuroanatomy, Department of Neuroscience, Yamaguchi University Graduate School of Medicine, 1-1-1 Mianmi-Kogushi, Ube, Yamaguchi 755-8505, Japan
[11]Large Scale Data Managing Unit, RIKEN Center for Integrative Medical Sciences, 1-7-22 Suehiro-cho, Tsurumi-ku, Yokohama, Kanagawa 230-0045, Japan
[12]School of Electrical Engineering and Computer Science, Queensland University of Technology, GPO Box 2434, Brisbane, QLD 4001, Australia
[13]Animal Resource Development Unit and Genetic Engineering Team, RIKEN Center for Biosystems Dynamics Research, 2-2-3 Minatojima Minami-machi, Chuo-ku, Kobe, Hyogo 650-0047, Japan
[14]These authors contributed equally
[15]Lead Contact
*Correspondence: uedah-tky@umin.ac.jp
https://doi.org/10.1016/j.celrep.2018.07.082

SUMMARY

Sleep regulation involves interdependent signaling among specialized neurons in distributed brain regions. Although acetylcholine promotes wakefulness and rapid eye movement (REM) sleep, it is unclear whether the cholinergic pathway is essential (i.e., absolutely required) for REM sleep because of redundancy from neural circuits to molecules. First, we demonstrate that synaptic inhibition of *TrkA*+ cholinergic neurons causes a severe short-sleep phenotype and that sleep reduction is mostly attributable to a shortened sleep duration in the dark phase. Subsequent comprehensive knockout of acetylcholine receptor genes by the triple-target CRISPR method reveals that a similar short-sleep phenotype appears in the knockout of two Gq-type acetylcholine receptors *Chrm1* and *Chrm3*. Strikingly, *Chrm1* and *Chrm3* double knockout chronically diminishes REM sleep to an almost undetectable level. These results suggest that muscarinic acetylcholine receptors, *Chrm1* and *Chrm3,* are essential for REM sleep.

INTRODUCTION

Acetylcholine was the first identified neurotransmitter (Dale, 1937), and the cholinergic system is one of the most extensively studied regulatory systems for mammalian sleep (Brown et al., 2012). The pioneering studies reported that pathological damages to the brain regions, which later appeared to be major cholinergic sources, resulted in sleep disorders (Economo, 1930; McGinty and Sterman, 1968; Nauta, 1946). The discovery of the regulatory site for rapid eye movement (REM) sleep in the brainstem (Jouvet, 1962) was affirmed by the induction of REM-sleep-like state by cholinergic agonists injected into the site (Cordeau et al., 1963; George et al., 1964). Therefore, the long-standing model of the transition from non-rapid eye movement (NREM) sleep to REM sleep incorporated acetylcholine as a key factor (Hobson et al., 1975; McCarley, 2004). In addition, acetylcholine release was found to be abundant in the brainstem during REM sleep (Kodama et al., 1990) and in the cortex during REM sleep and wakefulness (Teles-Grilo Ruivo et al., 2017). Despite this evidence, it is unclear whether cholinergic regulation is essential, i.e., required, for REM sleep, because multilayer complexity from neural circuits to molecules may compensate for perturbation of the cholinergic system at any one level. For example,

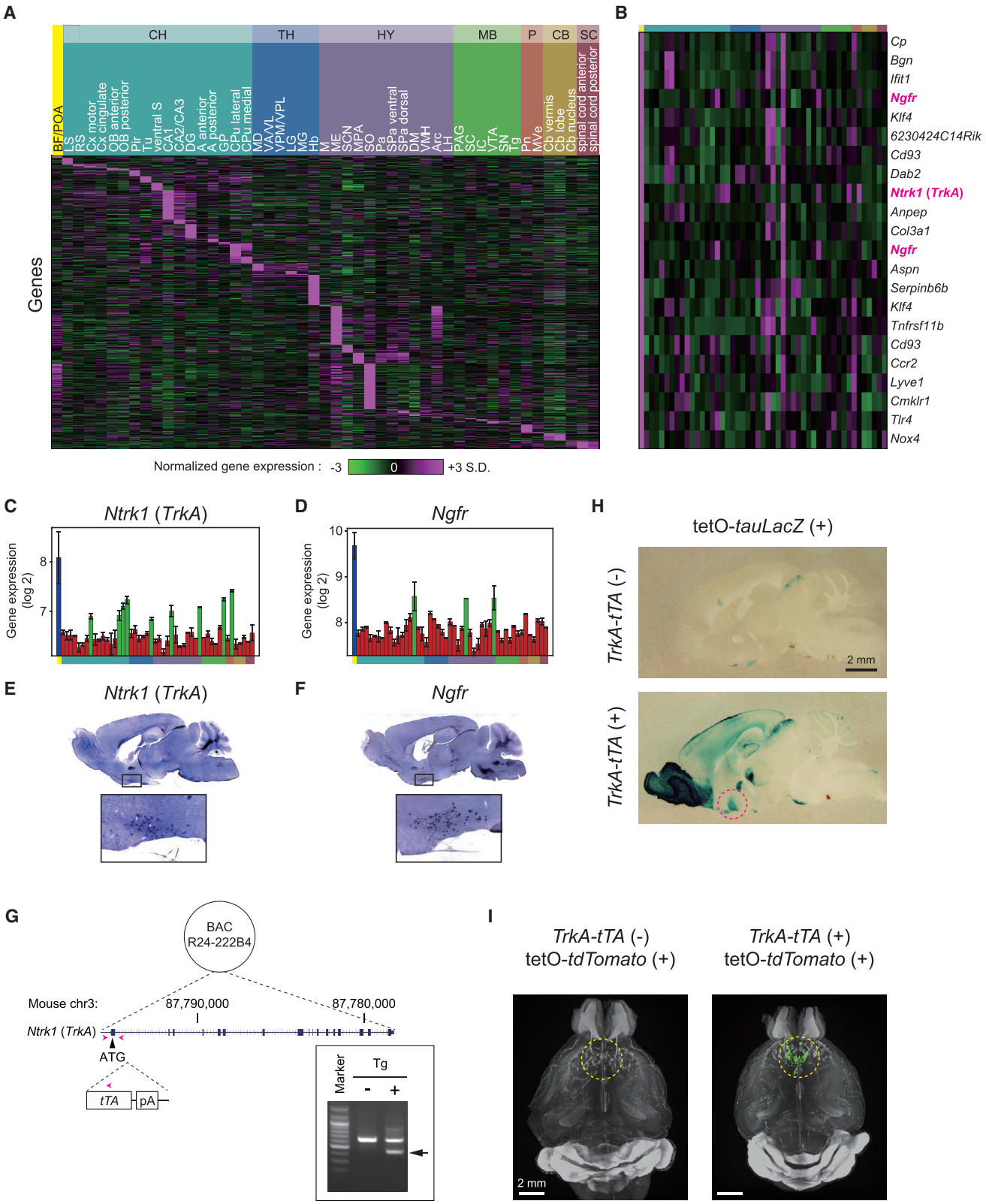

(legend on next page)

cholinergic neurons in the basal forebrain (BF) and regions of the brainstem, including the laterodorsal tegmentum (LDT) and the pedunculopontine tegmentum (PPT), are crucial for REM sleep (McCarley, 2004), but lesioning each of those cholinergic sites results in relatively minor effects (Brown et al., 2012), emphasizing the need for further neuronal subtyping to untangle the spatially intermingled circuits (Chung et al., 2017; Hayashi et al., 2015; Weber and Dan, 2016; Xu et al., 2015). In addition, there are eleven mammalian neuronal-type nicotinic acetylcholine receptors, and five muscarinic acetylcholine receptors (Gotti and Clementi, 2004; Wess, 2004), which results in considerable redundancy that hinders the identification of critical cholinergic receptors. Although *in vivo* pharmacological manipulations demonstrated that muscarinic acetylcholine receptors are important for the regulation of REM sleep (Brown et al., 2012), genetic approaches to assess the contribution of muscarinic acetylcholine receptors have been limited (Goutagny et al., 2005), and it is unknown which muscarinic receptors are particularly important and whether they are indispensable for the regulation of REM sleep.

To investigate these complexities, we took comprehensive genetic approaches to evaluate the role of cholinergic molecular factors in mice. First, we established a neuronal subtype of cholinergic neurons by finding enriched expression of the *neurotrophic receptor tyrosine kinase 1* (*Ntrk1*) (also called *TrkA*) gene and its potential co-receptor *nerve growth factor receptor* (*Ngfr*) in the brain region encompassing the basal forebrain. Temporally controlled synaptic inhibition of *TrkA*-expressing (*TrkA*+) and *Ngfr*-expressing (*Ngfr*+) neurons demonstrated that those neurons were crucial for sleep. Interestingly, the short-sleep phenotype caused by inhibition of *TrkA*+ and *Ngfr*+ neurons was associated with consolidated wakefulness in the dark phase, rendering the daily sleep profile more biphasic rather than the polyphasic profile naturally seen in mice and rats. Next, we identified the acetylcholine receptors whose inhibition recapitulates the characteristic short-sleep profile observed by inhibition of *TrkA*+ and *Ngfr*+ neurons. We knocked out most acetylcholine receptor genes identified in mice by a triple-target CRISPR method (Sunagawa et al., 2016) and found that loss of two Gq-type muscarinic acetylcholine receptors—*Chrm1* and *Chrm3*—induced the characteristic short-sleep profile. Both single knockouts of *Chrm1* and *Chrm3* reduced NREM sleep and reduced and fragmented REM sleep, respectively. Double-knockout of *Chrm1* and *Chrm3* diminished REM sleep to an almost undetectable level. These findings suggested that muscarinic acetylcholine receptors *Chrm1* and *Chrm3* are essential for sleep regulation, especially for REM sleep, and function in different ways.

RESULTS

Synaptic Inhibition of *TrkA*-Positive Neurons by Tetanus Toxin Induced a Characteristic Short-Sleep Phenotype with Consolidated Wake in the Dark Phase

For subtyping neurons in the BF/preoptic area (POA) regions, which have been shown to be important for sleep regulation (Brown et al., 2012), we performed genome-wide mRNA expression profiling of the BF and/or POA region along with data from 48 other brain regions in the BrainStars database (Figures 1A and S1A; Kasukawa et al., 2011). We found 22 candidate marker genes that were significantly enriched in the sampled BF and/or POA region (Figure 1B). Among them, we focused on *TrkA* and *Ngfr*, because NGF was implicated in the regulation of sleep (Ramos et al., 2011) and the majority of *TrkA*+ neurons in the BF and/or POA region coexpress *choline acetyltransferase* (*ChAT*) (Sobreviela et al., 1994; Figures 1B–1F). To examine the function of *TrkA*+ neurons, we first established *TrkA-tTA* bacterial artificial chromosome (BAC)-Tg mice and confirmed that the *TrkA-tTA*-driven gene was expressed in the BF and/or POA region by crossing *TrkA-tTA* mice with two independent reporter strains—tetO-*tdTomato* and tetO-*tauLacZ* mice (Li et al., 2010; Reijmers et al., 2007; Figures 1G–1I and S1B).

Then we crossed *TrkA-tTA* mice with tetO-*EGFP/TeNT* mice (Wada et al., 2007; Yamamoto et al., 2003) and produced double-transgenic *TrkA-TeNT* mice. In *TrkA-TeNT* mice, tetanus toxin (TeNT) is expressed and inhibits synaptic vesicle release in *TrkA*+ neurons under the control of Tet-off system. Shortly

Figure 1. The Tet-Driver Line for Subtyping the Cholinergic System Was Established based on Enriched Expression of *TrkA* and *Ngfr* Genes in the BF and/or POA Region

(A–D) Genome-wide mRNA expression profiles of BF and/or POA region analyzed along with data from 48 other brain regions, which we made public at the database (http://poabf.brainstars.org/).

(A) The mRNA expression profiles in 49 distinct brain regions are represented in a heatmap. Genes whose expression was enriched in one of those regions were selected from the genome-wide dataset. Each row corresponds to a gene and each column to a region designated at the top of the panel (see Figure S1 for the abbreviations).

(B) The expression profiles of candidate marker genes whose expression is most enriched in the BF and/or POA region.

(C and D) The mRNA expression profiles of *Ntrk1(TrkA)* (C) and *Ngfr* (D) across 49 brain regions. Blue bar represents the most enriched region, and green bars represent the second most enriched regions.

(E and F) *In situ* hybridization of mRNA of *Ntrk1(TrkA)* (E) and *Ngfr* (F). The POA/BF region is magnified in the lower panels.

(G) A schematic representation of the modified BAC DNA where *tTA* and *SV40* polyA signal were inserted just after the start codon of the *TrkA* gene. The genotype of BAC transgenic mice was confirmed by PCR (inset).

(H) The expression of a reporter gene driven by *TrkA-tTA* in the POA/BF region confirmed by crossing *TrkA-tTA* mice with tetO-*tauLacZ* mice. LacZ signal stained by X-gal was observed within the BF and/or POA region when both transgenes *TrkA-tTA* and tetO-*tauLacZ* were positive (bottom, dotted circle), but not observed when the *TrkA-tTA* was absent (top).

(I) The expression of a reporter gene driven by *TrkA-tTA* in the BF and/or POA region of the brain. The masked tdTomato signal is shown in the reconstituted 3D image for brains of tetO-*tdTomato(+);TrkA-tTA(−)* (left) and brains of tetO-*tdTomato(+);TrkA-tTA(+)* (right). Representative brains are shown. Gray dots represent nuclear signal of RedDot2; green dots represent cells in the 99 detected regions.

The scale bars represent 2 mm.

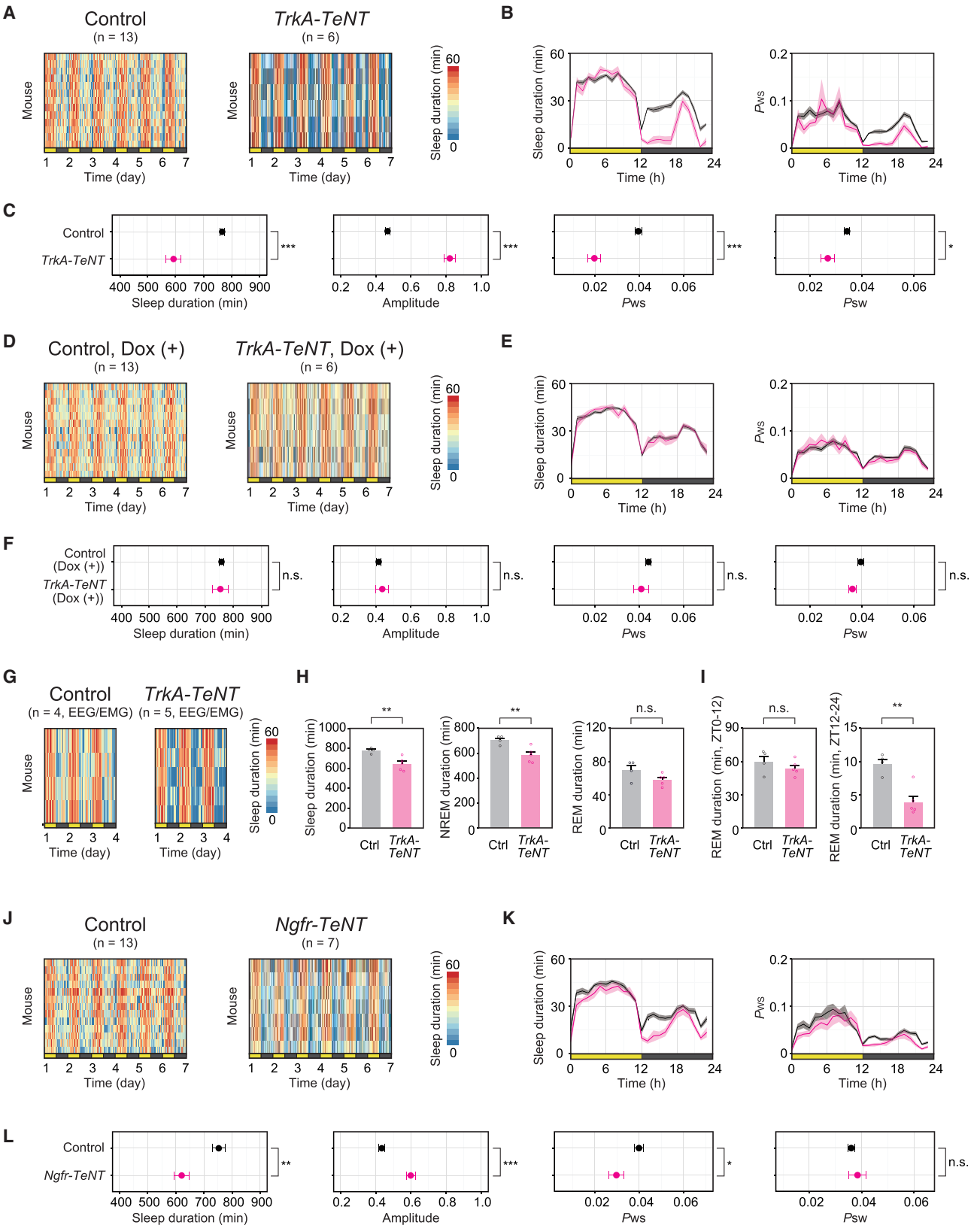

(legend on next page)

after birth, we provided mice with food containing 40 ppm doxycycline (dox-food) via their parental mother. After weaning and maturation with dox-food, we released mice to food without doxycycline (normal-food) and maintained mice for four weeks to allow for TeNT expression and inhibit *TrkA*+ neurons (from week 1 to week 4 in Figure S3A). We monitored the daily sleep profile using the non-invasive respiration-based automated sleep phenotyping system—snappy sleep stager (SSS) (Sunagawa et al., 2016)—and, at week 4 with normal-food, found a severe short-sleep phenotype of 593.0 ± 26.3 min (mean ± SEM; n = 6) of total sleep duration in a day, which was 173.0 min shorter than that of control littermates (n = 13; $p < 0.001$; Figures 2A–2C and S3A–S3D). Here, we used littermates as control that harbored only one or none of the two transgenes. Reduction of the sleep duration was mostly attributable to decreased P_{WS} (the transition probability from wakefulness to sleep), especially at night, hence consolidated wakefulness in the dark phase, which resulted in a high-amplitude variation in sleep duration (Figures 2B and 2C). This high-amplitude variation of *TrkA-TeNT* mice is apparent in the contrast between the light (resting) and the dark (active) phases in the time series of sleep duration represented by the heatmap (Figure 2A). In addition, there was a period of partially recovered sleep propensity at the late dark phase (Figure 2B). We confirmed that TeNT expression was induced in the BF and/or POA regions at week 2 and 3 by fluorescent *in situ* hybridization (FISH) analysis (Figures S4A and S4B). On and after week 5, we returned *TrkA-TeNT* mice to dox-food, and the characteristic short-sleep phenotype gradually weakened after one month and almost diminished three months later (week 16; Figures 2D–2F and S3A–S3D). We also confirmed that TeNT expression was not detected in the BF and/or POA regions at week 16 by FISH analysis (Figures S4A and S4B). These temporally controlled phenotypes were confirmed with different concentrations of doxycycline (Figures S3E–S3H).

Electroencephalogram (EEG) and electromyogram (EMG) recordings of sleep phenotypes of *TrkA-TeNT* mice recapitulated the characteristic short-sleep profile (Figure 2G), eliminating the possibility that *TrkA-TeNT* mice had an abnormality in the respiration system that might confound SSS recordings. Although the EEG power spectrum did not have a notable change (Figure S7D), sleep duration was 636.2 ± 29.8 min (mean ± SEM; n = 5), which was 134 min shorter than that of control littermates ($p < 0.01$; n = 4). The reduction was mostly attributable to a significant reduction of the duration of NREM sleep (Figure 2H). Although the duration of the REM sleep was not significantly changed over a day at 57.2 ± 3.2 min (mean ± SEM; n = 5) compared with that of the control littermates at 69.2 ± 5.9 min (mean ± SEM; n = 4; $p > 0.1$), focused in the dark phase, it was significantly reduced at 3.9 ± 1.0 min (mean ± SEM), which was 5.7 min shorter than that of the control littermates ($p < 0.01$; Figure 2I).

We also generated *Ngfr-TeNT* mice by crossing *Ngfr-tTA* mice (Figure S2D) with tetO-*EGFP*/*TeNT* mice. Both SSS analysis and EEG and EMG recordings revealed that they had the characteristic short-sleep profile with consolidated wake in the early dark phase (Figures 2J–2L, S2H, and S2I). Although the EEG power spectrum did not have a significant change (Figure S7E), the sleep duration measured by SSS was 620.9 ± 26.5 min (mean ± SEM; n = 7), which was 132 min shorter than that of control littermates ($p < 0.01$; n = 13; Figures 2J–2L). Furthermore, without temporal dox administration, the characteristic sleep phenotype was also observed in both *TrkA-TeNT* and *Ngfr-TeNT* mice (Figures S2A–S2C and S2E–S2G).

In addition, inhibition of *TrkA*+ neurons in circadian-clock-deficient mice (*Per1/2* double-knockout [DKO] mice; Bae et al., 2001) demonstrated that the function of *TrkA*+ neurons does not require a functional circadian clock (Figures S2J–S2O), excluding the possibility that *TrkA*+ neurons might have a role in the circadian process (process C) of the two-process model (Borbély, 1982).

Figure 2. Inhibition of the *TrkA*- and *Ngfr*-Expressing Neurons Induced a Characteristic Short-Sleep Phenotype with Consolidated Wakefulness in the Dark Phase

(A–C) Sleep phenotypes of *TrkA-TeNT* mice (n = 6) and control littermates with normal-food (n = 13) measured by the non-invasive respiration-based automated sleep phenotyping system—snappy sleep stager (SSS).

(A) Heatmap representation of sleep duration (per hour) over 6 days.

(B) The profile of sleep duration and P_{WS} (per hour) over 24 hr averaged over 6 days. The mean at each hour of the day is plotted for *TrkA-TeNT* mice (magenta line) and for control mice (black line). Shaded area around the line represents SEM.

(C) Sleep and wake parameters. Sleep duration is the total sleep duration in a day, amplitude is related to the variation of sleep duration (per hour) within the daily sleep cycle, and P_{WS} and P_{SW} are the respective transition probabilities from wakefulness to sleep and vice versa.

(D–F) Sleep phenotypes of the doxycycline (dox)-treated *TrkA-TeNT* mice (n = 6) and control littermates (n = 13) measured by SSS.

(D) Heatmap representation of sleep duration (per hour) over 6 days.

(E) The profile of sleep duration and P_{WS} (per hour) over 24 hr averaged over 6 days. The mean at each hour of the day is plotted for *TrkA-TeNT* mice (magenta line) and for control mice (black line). Shaded area represents SEM.

(F) Sleep and wake parameters are presented as in (C).

(G–I) Sleep phenotypes of *TrkA-TeNT* mice (n = 5) and control littermates (n = 4) measured by EEG and EMG recording.

(G) Heatmap representation of sleep duration (per hour) over 3 days.

(H) The duration of total sleep, NREM sleep, and REM sleep in a day.

(I) The duration of REM sleep in the light (left) or dark phase (right).

(J–L) Sleep phenotypes of *Ngfr-TeNT* mice (n = 7) and control littermates (n = 13) measured by SSS.

(J) Heatmap representation of sleep duration (per hour) over 6 days.

(K) The profile of sleep duration and P_{WS} (per hour) over 24 hr averaged over 6 days. The mean at each hour of the day is plotted for *Ngfr-TeNT* mice (magenta line) and control littermates (black line). Shaded area represents SEM.

(L) Sleep and wake parameters are presented as in (C).

Error bars represent SEM. *$p < 0.05$; **$p < 0.01$; ***$p < 0.001$.

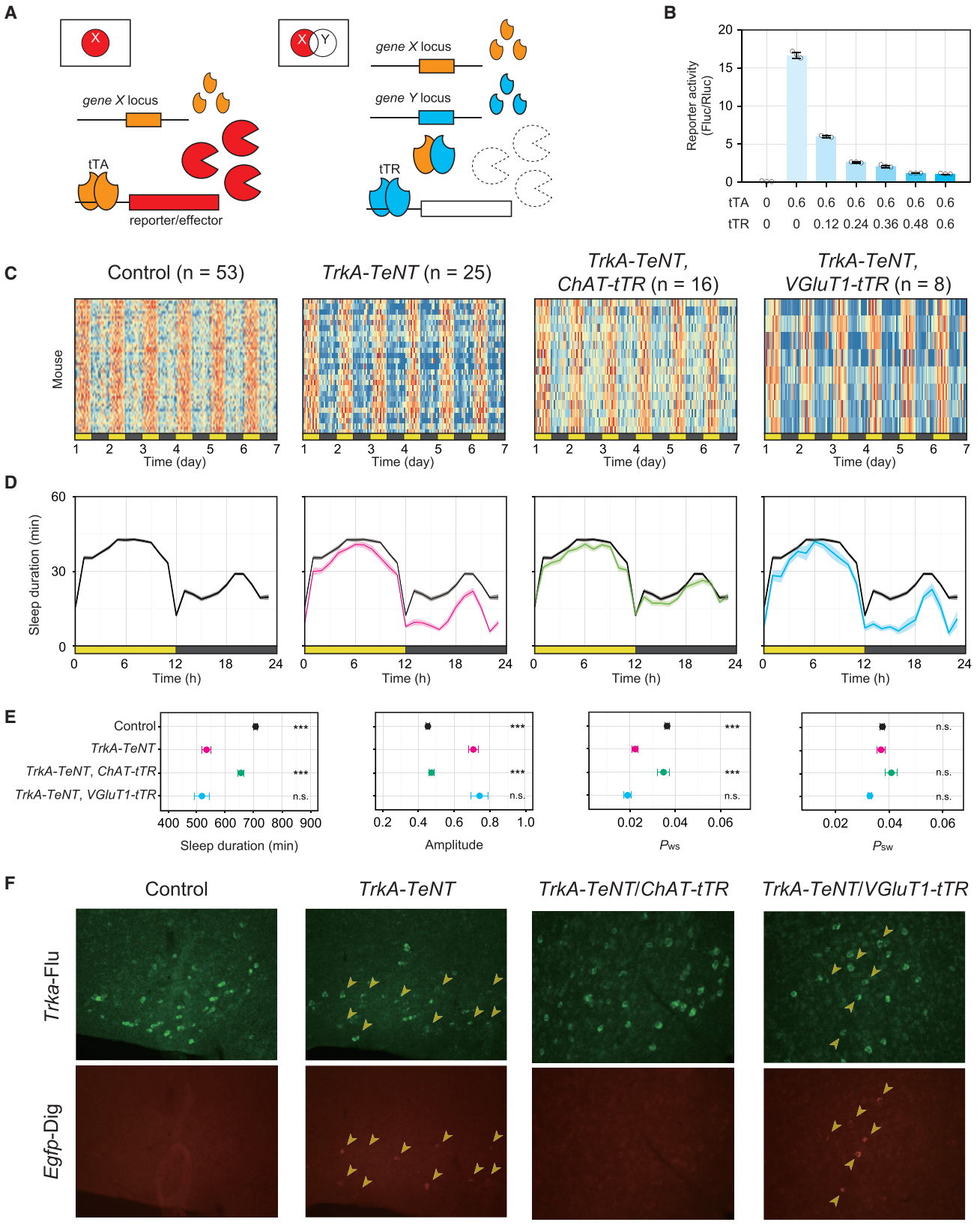

(legend on next page)

Together, these results suggested that *TrkA*- and *Ngfr*-expressing neurons regulate sleep in a way that promotes sleep.

Specific Rescue of *ChAT*-Positive Neurons in *TrkA-TeNT* Mice Restored Sleep Duration

The majority of *TrkA*+ neurons in the BF and/or POA region are cholinergic (Sobreviela et al., 1994), but *TrkA* expression was also found in non-cholinergic neurons in other brain regions, including the interpeduncular nucleus (IPN) (Holtzman et al., 1995), which is implicated in the regulation of REM sleep (Funato et al., 2010). To further characterize *TrkA*+ neurons that are responsible for the characteristic short-sleep phenotype of *TrkA-TeNT* mice, we designed a Tet effector tTR, which stands for tTA repressor. tTR inhibits tTA activity only when both are coexpressed in the same cells in a similar manner of *Gal80* and *Gal4* in fruit fly genetics (Figure 3A; Lee and Luo, 1999). In cultured cell analysis, tTR effectively repressed tTA-induced tetO-luciferase activity in a dose-dependent manner (Figure 3B). For *in vivo* application of tTR, we first established embryonic stem cells (ESCs) from *TrkA-TeNT* mice. Then we generated two different tTR knockin strains, *ChAT-tTR* and *VgluT1-tTR*, with *TrkA-TeNT* ESCs and the TALEN-based gene-targeting strategy (STAR Methods; Ode et al., 2017b; Ukai et al., 2017). In *TrkA-TeNT;VGluT1-tTR* mice, the characteristic short-sleep phenotype of *TrkA-TeNT* mice did not change (Figures 3C–3E). On the other hand, in *TrkA-TeNT;ChAT-tTR* mice, the short-sleep phenotype was mostly abolished (Figures 3C–3E). FISH analysis of those mice confirmed that TeNT expression was suppressed in *TrkA-TeNT;ChAT-tTR* mice, but not in *TrkA-TeNT;VGluT1-tTR* mice (Figure 3F). Furthermore, we generated *VGluT1-tTR* or *ChAT-tTR* single-knockin mice and confirmed that tTR and either *VGluT1* or *ChAT* was coexpressed by FISH (Figures S4C and S4D). These results suggested the *TrkA*+ cholinergic neurons are primarily responsible for the characteristic phenotype observed in *TrkA-TeNT* mice (Figures 2A–2C).

Comprehensive Analysis of Nicotinic Acetylcholine Receptor KO Mice Showed Moderate Effects

After we discovered that *TrkA*+ cholinergic neurons have a crucial role in the regulation of sleep, we sought to elucidate the function of cholinergic receptors by comprehensively examining the phenotypes of acetylcholine receptor knockout (KO) mice.

There are two different families of acetylcholine receptors—nicotinic receptors and muscarinic receptors. Nicotinic acetylcholine receptors (nAchR) consist of five types of subunits—alpha (α1–10), beta (β2–5), delta, epsilon, and gamma. These subunits can be divided into the muscle type and neuronal type. We focused on the mammalian neuronal type and targeted eleven genes—*Chrna2*, *Chrna3*, *Chrna4*, *Chrna5*, *Chrna6*, *Chrna7*, *Chrna9*, *Chrna10*, *Chrnb2*, *Chrnb3*, and *Chrnb4* (Gotti and Clementi, 2004). To efficiently produce KO mice of each gene, we used a triple-target CRISPR method (STAR Methods). The genotype of KO mice was confirmed by qPCR (Figure S5; Table S2). KO of *Chrna3* was lethal because mice died shortly after birth (n = 26), which was consistent with the result of the conventional KO method (Xu et al., 1999). Among the KO mice, *Chrnb2* KO had a sleep profile resembling that of *TrkA-TeNT* mice (Figures 4A–4C and 2A–2C), but changes in sleep and wake parameters, including sleep duration, amplitude, and P_{WS}, were not significant within the statistical power achieved by availability of the mutant mice. Changes in other KO mice were weaker than those of *Chrnb2* KO, and none were significant (Figure 4C). *Chrnb3* KO mice (n = 8), which were obtained in an additional batch of KO mice production at different research site, had significant changes in amplitude and P_{WS}, but the change of sleep duration was moderate at 649.3 ± 13.5 min (mean ± SEM; n = 8), which was only 38.3 min shorter than that of wild-type (WT) mice (less than 0.76 SD; $p < 0.05$; n = 108; Figures 4D–4F). These results suggested that nicotinic acetylcholine receptors have relatively minor roles in the regulation of sleep.

Comprehensive Analysis of Muscarinic Acetylcholine Receptor KO Mice Revealed that *Chrm1* and *Chrm3* Are Important for Sleep Regulation

Therefore, we focused on muscarinic acetylcholine receptors (*mAchR*s), which are G-protein-coupled receptors comprising five members (*Chrm1*, *Chrm2*, *Chrm3*, *Chrm4*, and *Chrm5*; Wess, 2004), and comprehensively examined KO phenotypes

Figure 3. Rescue of Cholinergic Neurons in *TrkA-TeNT* Mice by the tTR System Mostly Abolished the Characteristic Short-Sleep Phenotype

(A) Schematic representation of the dual conditional expression pattern achieved by Tet system and the tTA repressor tTR. In Tet system, the reporter or effector expression is activated by tTA driven by promoter and/or enhancer of *geneX* (left) in the absence of dox. With tTR driven by promoter and/or enhancer of *geneY* as an inhibitor, the reporter or effector expression is suppressed in cells expressing both *geneX* and *geneY* (right).

(B) Luciferase assay in cultured cells showing the effect of tTR on tTA-induced tetO-luciferase (FLuc) activity. The x axis indicates the amount of DNA (μg) for tTA and tTR used in the experiment. *Renilla* luciferase (RLuc) was used as an internal control.

(C–E) Proof-of-concept experiments of tTR-rescue system *in vivo*. The sleep phenotypes of *TrkA-TeNT* mice (n = 25), *TrkA-TeNT;ChAT-tTR* mice (n = 16), *TrkA-TeNT;VGluT1-tTR* mice (n = 8), and control littermates (n = 53) were analyzed by SSS.

(C) Heatmap representation of sleep duration (per hour) over 6 days.

(D) The profile of sleep duration (per hour) over 24 hr averaged over 6 days. The mean sleep duration at each hour of the day is plotted for control littermates (black line in each panel) and for mutants, i.e., *TrkA-TeNT* mice (magenta line), *TrkA-TeNT;ChAT-tTR* mice (green line), and *TrkA-TeNT;VGluT1-tTR* mice (blue line). Shaded area represents SEM.

(E) Sleep and wake parameters. Sleep duration is the total sleep duration in a day, amplitude is related to the variation of the sleep duration (per hour) within the daily sleep cycle, and P_{WS} and P_{SW} are the respective transition probabilities from wakefulness to sleep and vice versa. *$p < 0.05$; **$p < 0.01$; ***$p < 0.001$ by the Steel test against *TrkA-TeNT*.

(F) Repressed expression of tetanus toxin (*TeNT*) by tTR. *TrkA* (fluorescein labeled, Flu; green) and *TeNT* expression were measured by fluorescent *in situ* hybridization (FISH). *TeNT* expression was measured by an antisense RNA probe against *Egfp* fused to *TeNT* (digoxigenin labeled, Dig: red).

Error bars represent SEM.

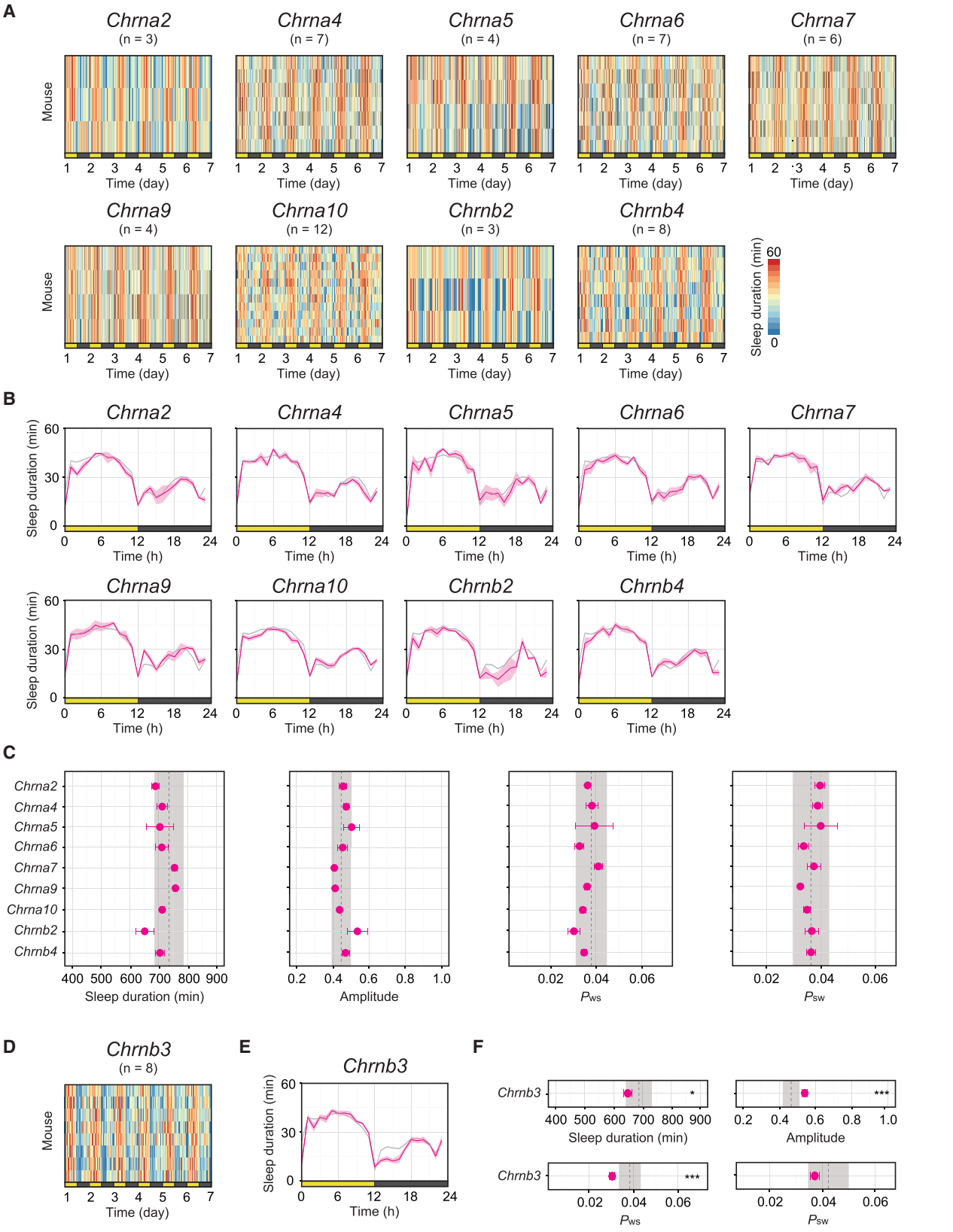

(legend on next page)

with a triple-target CRISPR method (STAR Methods; Figure S6; Table S2). Interestingly, KO mice of two Gq-type muscarinic acetylcholine receptors, *Chrm1* KO and *Chrm3* KO, had the characteristic short-sleep profile with consolidated wake in the early dark phase, which resembled the sleep profile of *TrkA-TeNT* mice (Figures 5A–5C and 2A–2C). Sleep duration was decreased to 642.3 ± 25.5 min in *Chrm1* KO mice (mean ± SEM; n = 8) and 607.0 ± 7.0 min in *Chrm3* KO mice (mean ± SEM; n = 11), which was 82.4 min and 117.7 min shorter, respectively, ($p < 0.01$ and more than 1.85 SD for *Chrm1* and $p < 0.001$ and more than 2.64 SD for *Chrm3*) compared to that of WT mice (n = 108).

To preclude the possibility of off-target effects of the CRISPR guide RNAs used for producing *Chrm1* KO and *Chrm3* KO mice (set 1 in Figures 5A–5C and S6), we produced another group of KO mice using independent CRISPR guide RNAs (set 2; Figure S6) and confirmed the observed characteristic short-sleep phenotypes (Figures 5D–5G). These results strongly suggested that the observed short-sleep phenotype of *Chrm1* and *Chrm3* KO mice cannot be attributed to the possible off-target effects of CRISPR but rather to the common genomic defects in the *Chrm1* and *Chrm3* genes, respectively. Importantly, the observed reduction of sleep duration in *Chrm1* KO mice (set 2) and *Chrm3* KO mice (set 2) was mostly attributable to the decreased P_{WS} in the early dark phase (Figures 5F and 5G), which was also observed in *Chrm1* KO mice (set 1) and *Chrm3* KO mice (set 1; Figures 5B and 5C) as well as in *TrkA-TeNT* mice (Figures 2B and 2C).

Chrm3 KO Reduced the Duration of NREM Sleep and Fragmented REM Sleep

To further ensure that the characteristic short-sleep phenotype was not because of an artifact of sleep evaluation by the respiration-based SSS, we performed EEG and EMG recordings of *Chrm1* and *Chrm3* KO mice (set 1) used in the previous measurement (Figures 5A–5C) and confirmed the characteristic sleep profile with consolidated wake in the dark phase (Figures 6A, 6D, and 6G). Interestingly, EEG and EMG revealed that *Chrm1* KO and *Chrm3* KO mice had different sleep architectures (Figures 6B and 6E). Notably, the power spectrum of *Chrm3* KO mice displayed increased power both in the delta (0.5–4 Hz) and theta (6–10 Hz) domains in sleep, implying that the synchrony of cortical neurons was increased at those frequency domains in *Chrm3* KO mice (Figures S7A and S7B).

In *Chrm3* KO mice, the duration of NREM sleep in a day was significantly reduced at 542.9 ± 16.5 min, which was 152.5 min shorter than that of WT mice (n = 6; $p < 0.001$), but the duration of REM sleep in a day did not significantly change at 73.7 ± 4.4 min compared with that of WT mice ($p = 0.86$; Figure 6E). The reduction of the duration of NREM sleep was attributable to decreased P_{WN} (the transition probability from wakefulness to NREM sleep) and increased P_{WW} (the transition probability from wakefulness to wakefulness or the probability of staying in wakefulness), especially in the dark phase (Figures 6F and 6G; Table S3). The duration of REM sleep did not significantly change (Table S3). However, the transition probabilities between REM sleep and NREM sleep (P_{RN} and P_{NR}) were mutually increased (Figure 6F), especially in the light phase (Figure 6G). The increased transition with the retained total duration of REM sleep indicated that REM sleep was fragmented, and hence, P_{RR} (the transition probability from REM sleep to REM sleep or the probability of staying in REM sleep) was decreased (Figure 6F), resulting in the reduced episode duration of REM sleep (Table S3C). Together, these observations suggested that *Chrm3* has a role in regulating the duration of NREM sleep in a day but also contributes to the consolidation of REM sleep.

Chrm1 KO Reduced the Duration of REM Sleep

In contrast to *Chrm3* KO mice that retained the duration of REM sleep in a day, *Chrm1* KO mice had a significantly decreased duration of REM sleep in a day at 47.4 ± 4.8 min, which was 33.6 min shorter than that of WT mice (n = 7; $p < 0.001$; Figures 6B and 6E; Table S3). The reduction in the duration of REM sleep was accounted for by an increased P_{RN} (the transition probability from REM sleep to NREM sleep), implying weakened maintenance of REM sleep (Figures 6C and 6G; Table S3). Although not as much as *Chrm3* KO mice, *Chrm1* KO mice also had a significant reduction in the duration of NREM sleep at 612.6 ± 23.6 min, which was 116.8 min shorter than that of WT mice (n = 7; $p < 0.001$). The reduction of the duration of NREM sleep was mostly attributable to reduced P_{WN} and increased P_{WW}, especially in the dark phase (Figures 6C and 6G; Table S3), which resulted in the characteristic short-sleep profile with consolidated wakefulness in the dark phase as was observed

Figure 4. Comprehensive Analysis of Sleep Phenotypes by Triple-Target CRISPR KO Revealed a Minor Effect from Nicotinic Receptors

(A–C) Sleep phenotypes measured by SSS for the series of KO mice of nine nicotinic acetylcholine receptors: *Chrna2* (n = 3); *Chrna4* (n = 7); *Chrna5* (n = 4); *Chrna6* (n = 7); *Chrna7* (n = 6); *Chrna9* (n = 4); *Chrna10* (n = 12); *Chrnb2* (n = 3); and *Chrnb4* (n = 8).

(A) Heatmap representation of sleep duration (per hour) over 6 days.

(B) The profile of sleep duration (per hour) over 24 hr averaged over 6 days. The mean sleep duration at each hour of the day is plotted for KO mice (magenta line) and for the C57BL/6N wild-type mice (gray line; n = 108; replotted from the previous report; Sunagawa et al., 2016). The shaded area represents SEM.

(C) Sleep and wake parameters. Sleep duration is the total sleep duration in a day, amplitude is related to the variation of the sleep duration (per hour) within the daily sleep cycle, and P_{WS} and P_{SW} are the respective transition probabilities from wakefulness to sleep and vice versa. The black dashed line and the shaded area represent the mean and 1 SD range of the wild-type control mice, respectively.

(D–F) Sleep phenotypes of *Chrnb3* KO mice (n = 8) measured by SSS.

(D) Heatmap representation of sleep duration (per hour) over 6 days.

(E) The profile of sleep duration (per hour) over 24 hr averaged over 6 days. The mean sleep duration at each time of the day is plotted for *Chrnb3* KO mice (magenta line) and for C57BL/6N wild-type (gray line; n = 107). The shaded area represents SEM.

(F) The sleep and wake parameters are presented as in (C).

Error bars represent SEM. *$p < 0.05$; **$p < 0.01$; ***$p < 0.001$.

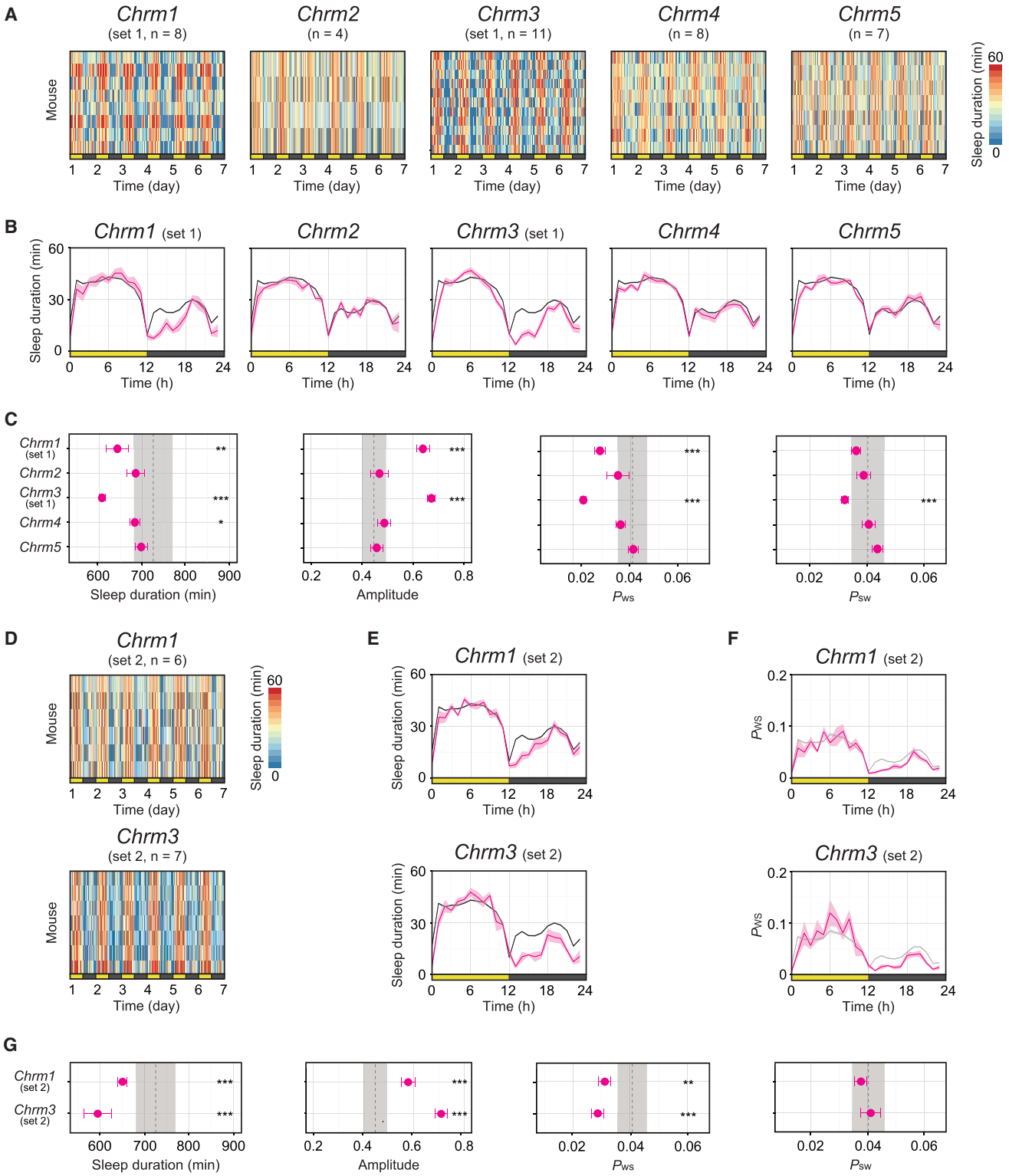

Figure 5. Comprehensive Analysis of Sleep Phenotypes by Triple-Target CRISPR KO Revealed Prominent Effects of Two Muscarinic Acetylcholine Receptors *Chrm1* and *Chrm3*

(A–C) Sleep phenotypes measured by SSS for the series of KO mice of five muscarinic acetylcholine receptors: *Chrm1* (set 1; n = 8); *Chrm2* (n = 4); *Chrm3* (set 1; n = 11); *Chrm4* (n = 8); and *Chrm5* (n = 7).

(A) Heatmap representation of sleep duration (per hour) over 6 days. Set 1 indicates the guide (gRNAs) used for producing the mutant mice.

(legend continued on next page)

in *Chrm3* KO mice (Figures 6A and 6G). These observations suggested that *Chrm1* has a role in regulating the duration of REM sleep but also contributes to the duration of NREM sleep.

Chrm1 and *Chrm3* Are Essential for REM Sleep and Important for NREM Sleep

Compared to *TrkA-TeNT* mice, changes in sleep phenotype, especially changes in amplitude and P_{WS}, of *Chrm1* KO mice and *Chrm3* KO mice were moderate (Figures 5G and 2C; Table S3). To examine the combinatorial effect of *Chrm1* and *Chrm3* for sleep, we produced *Chrm1* and *Chrm3* double-KO mice (*Chrm1/3* dKO mice) by triple-target CRISPR (set 1/set 1; Figure S6O) and measured phenotypes using SSS (Figures 6H–6J). *Chrm1/3* double-KO mice had changes in sleep duration, amplitude, and P_{WS} to a degree comparable to that of *TrkA-TeNT* mice (Figures 6I, 6J, 2B, and 2C; Table S3). In *Chrm1/3* double-KO mice, sleep duration in a day was reduced to 591.1 ± 16.8 min (mean ± SEM; n = 5), which was 133.6 min shorter, amplitude was increased, and P_{WS} was decreased compared to that of control mice (n = 108; $p < 0.001$ and more than 2.85 SD for the sleep duration; $p < 0.001$ for amplitude; $p < 0.001$ for P_{WS}; Figures 6J and 2C; Table S3). Decreased P_{WS}, especially in the dark phase, resulted in the characteristic short-sleep profile with consolidated wakefulness in the early dark phase (Figure 6I). In addition, both *TrkA-TeNT* mice and *Chrm1/3* double-KO mice consistently exhibited the enhanced rebound sleep after sleep deprivation, which suggested that homeostatic sleep control remained functional in those mutant mice (Figures S7F–S7I).

We observed the phenotypes of *Chrm1/3* double-KO mice by EEG and EMG recordings, which confirmed the characteristic short-sleep phenotype with consolidated wakefulness in the dark phase (Figure 6K). Strikingly, dKO of *Chrm1* and *Chrm3* diminished REM sleep to an almost undetectable level (Figure 6L; Table S3). We did not find any overt abnormality resembling those found in REM behavior disorder (RBD) (Krenzer et al., 2011; Lu et al., 2006) by visual inspection of recorded video at timing of EEG theta-oscillation dominant period. We also checked transition periods from NREM sleep to wakefulness, which might contain REM sleep masked by RBD, and did not find any abnormality (Krenzer et al., 2011; Lu et al., 2006). Although the interruption of REM sleep by abnormal behaviors could increase the transition probability from REM sleep to wakefulness (P_{RW}) by conventional EEG analysis, P_{RW} did not exhibit any marked increase either in *Chrm1* and *Chrm3* single-KO mice (Figures 6C and 6F), which supports the claim that RBD is not masking REM sleep in *Chrm1/3* double-KO mice. Interestingly, the hypnograms showed that there is virtually no emergence of typical polygraphic manifestation of REM sleep, that is, a lasting low-delta power and low muscle tone in the *Chrm1/3* double-KO mice (Figure 7C). In line with this observation, the EEG power spectrum of *Chrm1/3* double-KO mice displayed reduced theta power in NREM sleep (Figure S7C).

To further ensure loss of REM sleep, we produced another group of *Chrm1/3* double-KO ESC mice by injecting CRISPR-edited ESCs into 8-cell stage embryos (Ode et al., 2017a; Ukai et al., 2017) and performed EEG and EMG recordings to evaluate the response of sleep deprivation in *Chrm1/3* double-KO ESC mice. *Chrm1/3* double-KO ESC mice were implanted with EEG and EMG probes, housed in a 12:12 hr light-dark cycle, and stimulated with the gentle touch of a brush to deprive sleep from zeitgeber time 6 (ZT6) to ZT12. REM sleep in *Chrm1/3* double-KO ESC mice was virtually not detected both before and after sleep deprivation, despite a rebound in total sleep (14.3% increase; $p < 0.01$ from 276.7 ± 11.4 min in basal duration to 316.2 ± 11.0 min in rebound duration) and rebound REM sleep (154.4% increase; $p < 0.001$ from 16.5 ± 2.8 min to 37.4 ± 1.3 min) in the control WT mice or rebound total sleep in *Chrm1/3* double-KO ESC mice (49.5% increase; $p < 0.05$ from 112.9 ± 16.1 min in basal duration to 168.8 ± 18.7 min in rebound duration; Figure 6M). These results demonstrated that two Gq-type muscarinic acetylcholine receptors *Chrm1* and *Chrm3* are essential for REM sleep.

DISCUSSION

Since the pioneering works of defining REM sleep based on EEG and EMG (Aserinsky and Kleitman, 1953; Dement and Kleitman, 1957) and demonstrating that neural circuits in the brainstem are necessary and sufficient for REM sleep generation (Jouvet, 1962), our knowledge on the neural circuitry for regulating REM sleep has been steadily advancing (Hayashi et al., 2015; Weber and Dan, 2016). However, the essential molecular factors for defining and translating the output of the brainstem circuit to the collective activity of cortical neurons have been elusive. Multiple lines of *in vivo* pharmacological evidence consistently indicated that muscarinic acetylcholine receptors are important for the regulation of REM sleep. Muscarinic receptor agonists and acetylcholinesterase inhibitors increase REM sleep and shorten REM latency (the delay of the onset of REM sleep to that of NREM sleep; Brown et al., 2012). Moreover, muscarinic receptor

(B) The profile of sleep duration (per hour) over 24 hr averaged over 6 days. The mean sleep duration at each hour of the day is plotted for KO mice (magenta line) and for the C57BL/6N wild-type mice (gray line; n = 108). The shaded area represents SEM.
(C) Sleep and wake parameters. Sleep duration is the total sleep duration in a day, amplitude is related to the variation of the sleep duration (per hour) within the daily sleep cycle, and P_{WS} and P_{SW} are the respective transition probabilities from wakefulness to sleep and vice versa. The black dashed line and shaded area represent the mean and 1 SD range of the wild-type control mice, respectively.
(D–G) Sleep phenotypes of another group of *Chrm1* (n = 6) or *Chrm3* (n = 7) KO mice produced by a different set of gRNAs (set 2).
(D) Heatmap representation of sleep duration (per hour) over 6 days.
(E) The profile of sleep duration (per hour) over 24 hr averaged over 6 days, as in (B).
(F) The profile of P_{WS} (per hour) over 24 hr averaged over 6 days. The mean P_{WS} at each hour of the day are plotted for KO (magenta line) and for C57BL/6N wild-type mice (gray; n = 108). The shaded area represents SEM.
(G) The sleep and wake parameters are presented as in (C).
Error bars represent SEM. *$p < 0.05$; **$p < 0.01$; ***$p < 0.001$.

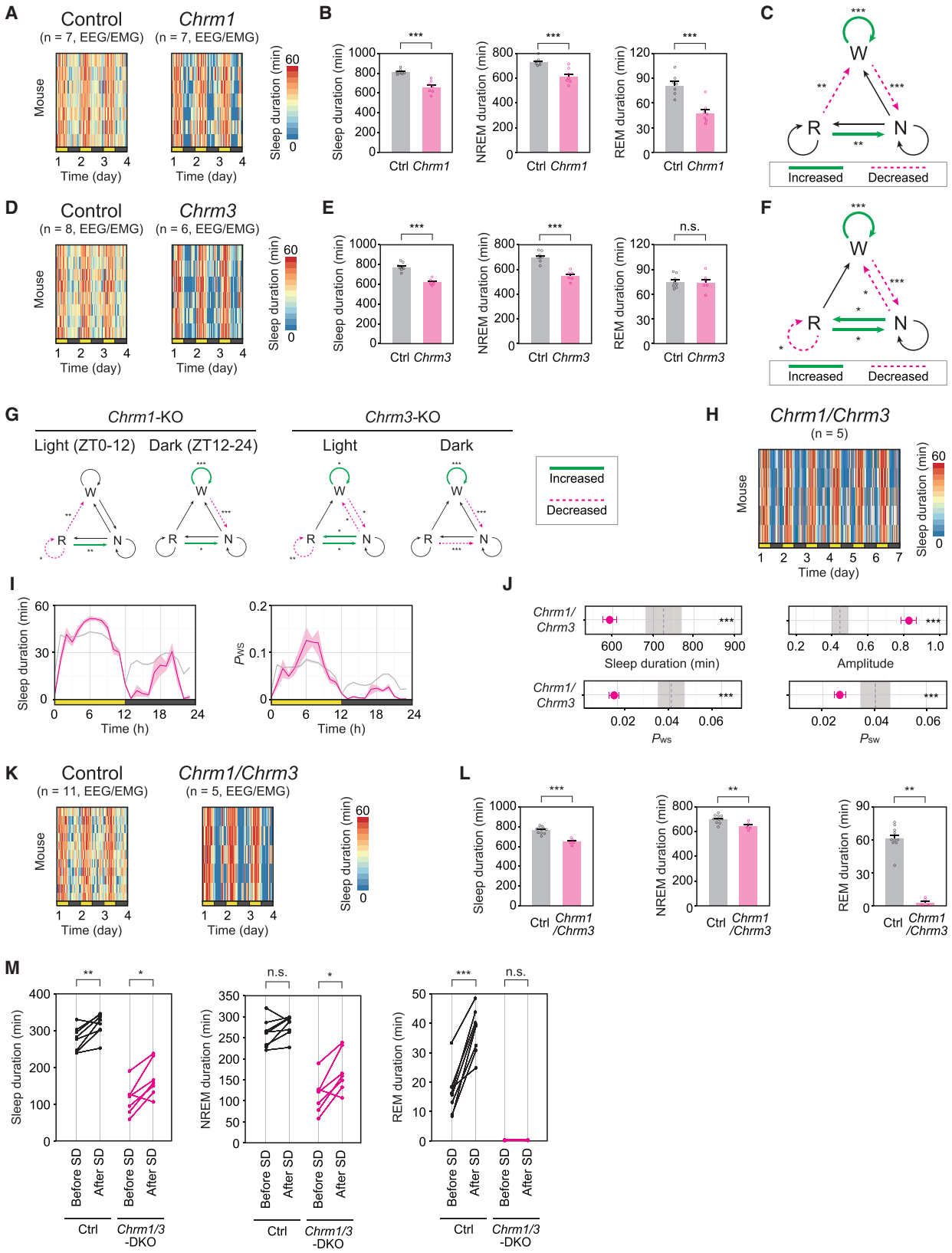

(legend on next page)

antagonists decrease REM sleep and lengthen REM latency (Brown et al., 2012). Nonetheless, genetic approaches to assess the contribution of muscarinic acetylcholine receptors to REM sleep regulation have been limited (Goutagny et al., 2005), and it is unknown which muscarinic acetylcholine receptors are required for the regulation of REM sleep. In the present study, our comprehensive genetic assays of acetylcholine receptors revealed that two Gq-type muscarinic acetylcholine receptors *Chrm1* and *Chrm3* of the five muscarinic acetylcholine receptors from *Chrm1* to *Chrm5* are important for REM sleep. KO of other Gq-type receptor *Chrm5* did not significantly change sleep phenotypes, which may reflect the low abundance of *Chrm5* in the brain. *Chrm1* and *Chrm3* are broadly expressed in different brain regions, including the cortex and the hippocampus, but *Chrm5* is expressed in relatively limited regions, such as the substantia nigra and the ventral tegmental area (VTA), in the midbrain (Basile et al., 2002; Buckley et al., 1988; Yasuda et al., 1993). *Chrm1/3* double-KO mice had an almost complete loss of REM sleep, which strongly suggested that *Chrm1* and *Chrm3* are essential for REM sleep.

In addition, the *Chrm1/3* double-KO mice exhibited the characteristic short-sleep profile with consolidated wakefulness in the early dark phase. This characteristic phenotype was also observed in *Chrm1* and *Chrm3* single-KO mice and in *TrkA-TeNT* mice. Reduction of sleep duration of all those mice was mostly attributable to the reduced duration of NREM sleep, indicating that cholinergic regulation is also important for NREM sleep. Impaired REM sleep might also reduce the duration of NREM sleep (Hayashi et al., 2015) because our observation indicated that the loss of either *Chrm1* (Figures 6B, 6C, 7A, and 7D), *Chrm3* (Figures 6E, 6F, 7B, and 7E), or both (Figures 6L, 7C, and 7F) resulted in reduced, fragmented, and diminished REM sleep, respectively. However, the question of how cholinergic pathways regulate NREM sleep remains unresolved (Figure 7G). Recent optogenetic and pharmacogenetic studies suggested that cholinergic neurons promote wakefulness at the circuit level (Chen et al., 2016; Shi et al., 2015; Xu et al., 2015; Zant et al., 2016), whereas our results indicated that cholinergic regulation suppresses wakefulness at the systems level. This apparent inconsistency may be reconciled by hypothesizing muscarinic modulation of other neurotransmitter systems, such as glutamatergic neurons (Kamsler et al., 2010; Weng et al., 2014) and GABAergic neurons (Xiao et al., 2009), or by hypothesizing the proximal projection of *TrkA*+ neurons to sleep-promoting neurons, such as POA GABAergic neurons, that inhibit wake-promoting neurons in the tuberomammillary histaminergic neurons (TMNs) (Chung et al., 2017). Indeed, a specific cholinergic receptor could be sleep-promoting although overall effect of the cholinergic system is wake promoting, as reported for the redeye mutant in *Drosophila*, where REM sleep has so far not been identified (Shi et al., 2014), implying the sleep-promoting cholinergic effect might be independent of REM sleep (Figure 7G).

Our findings of the essential role of *Chrm1* and *Chrm3* genes in REM sleep will provide useful tools in future studies of REM sleep. In particular, the finding of unexpected viability despite the almost completely abolished REM sleep will allow us to rigorously verify whether REM sleep plays crucial roles in fundamental functions of organism, such as learning and memory (Crick and Mitchison, 1983; Dement et al., 1967; Li et al., 2017), and open a way to study its underlying molecular and cellular mechanisms.

STAR★METHODS

Detailed methods are provided in the online version of this paper and include the following:

- KEY RESOURCES TABLE
- CONTACT FOR REAGENT AND RESOURCE SHARING
- EXPERIMENTAL MODEL AND SUBJECT DETAILS

Figure 6. *Chrm1* and *Chrm3* Have Differential Roles for NREM and REM Sleep and Are Essential for REM Sleep

(A–F) Sleep phenotype of *Chrm1* or *Chrm3* KO mice measured by EEG and EMG recordings.

(A) Heatmap representation of sleep duration (per hour) over 3 days for *Chrm1* KO (set 1; n = 7) and control (C57BL/6N) mice (n = 7).

(B) The durations of total sleep, NREM sleep, and REM sleep.

(C) The changes in transition probability among wakefulness, NREM sleep, and REM sleep are presented for *Chrm1* KO mice. The green bold and magenta dotted lines represent a significant increase and decrease, respectively, compared to that of control mice.

(D) Heatmap representation of sleep duration (per hour) over 3 days for *Chrm3* KO (set 1; n = 6) and control (C57BL/6N) mice (n = 8).

(E) The durations of total sleep, NREM sleep, and REM sleep.

(F) The changes in transition probability among wakefulness, NREM sleep, and REM sleep are presented for *Chrm3* KO mice as in (C).

(G) The changes in transition probabilities among wakefulness, NREM sleep, and REM sleep in the light phase (ZT0–12) and dark phase (ZT12–24) for *Chrm1* or *Chrm3* KO mice used in (A) and (D).

(H–J) Sleep phenotype of *Chrm1* and *Chrm3* double-KO mice (*Chrm1/3* double-KO mice; set 1/set 1; n = 5) measured by SSS.

(H) Heatmap representation of sleep duration (per hour) over 6 days.

(I) The profile of sleep duration and P_{WS} (per hour) over 24 hr averaged over 6 days. The mean at each hour of the day for the KO mice (magenta line) and for C57BL/6N wild-type mice (gray line; n = 108) is shown. The shaded area represents SEM.

(J) The sleep and wake parameters. Sleep duration is the total sleep duration in a day, amplitude is related to the variation of the sleep duration (per hour) within the daily sleep cycle, and P_{WS} and P_{SW} are the respective transition probabilities from wakefulness to sleep and vice versa. The black dashed line and the shaded area represent the mean and 1 SD range of the control, respectively.

(K and L) Sleep phenotypes of *Chrm1/3* double-KO mice (n = 5) and control mice (n = 11) measured by EEG and EMG recordings.

(K) Heatmap representation of sleep duration (per hour) over 6 days for *Chrm1/3* DKO and control (C57BL/6N) mice.

(L) The durations of total sleep, NREM sleep, and REM sleep.

(M) The sleep duration of total sleep, NREM sleep, and REM sleep measured by EEG and EMG recordings in the 12 hr before and after sleep deprivation (SD). "After SD" and "before SD," respectively, correspond to the sleep duration of ZT12–24 subsequent to SD and the sleep duration of ZT12–24 in the day before the day of SD. SD was applied for *Chrm1/3* double-KO ESC mice (n = 7) and control (C57BL/6N) mice (n = 8) for 6 hr from ZT6 to ZT12.

Error bars represent SEM. *p < 0.05; **p < 0.01; ***p < 0.001.

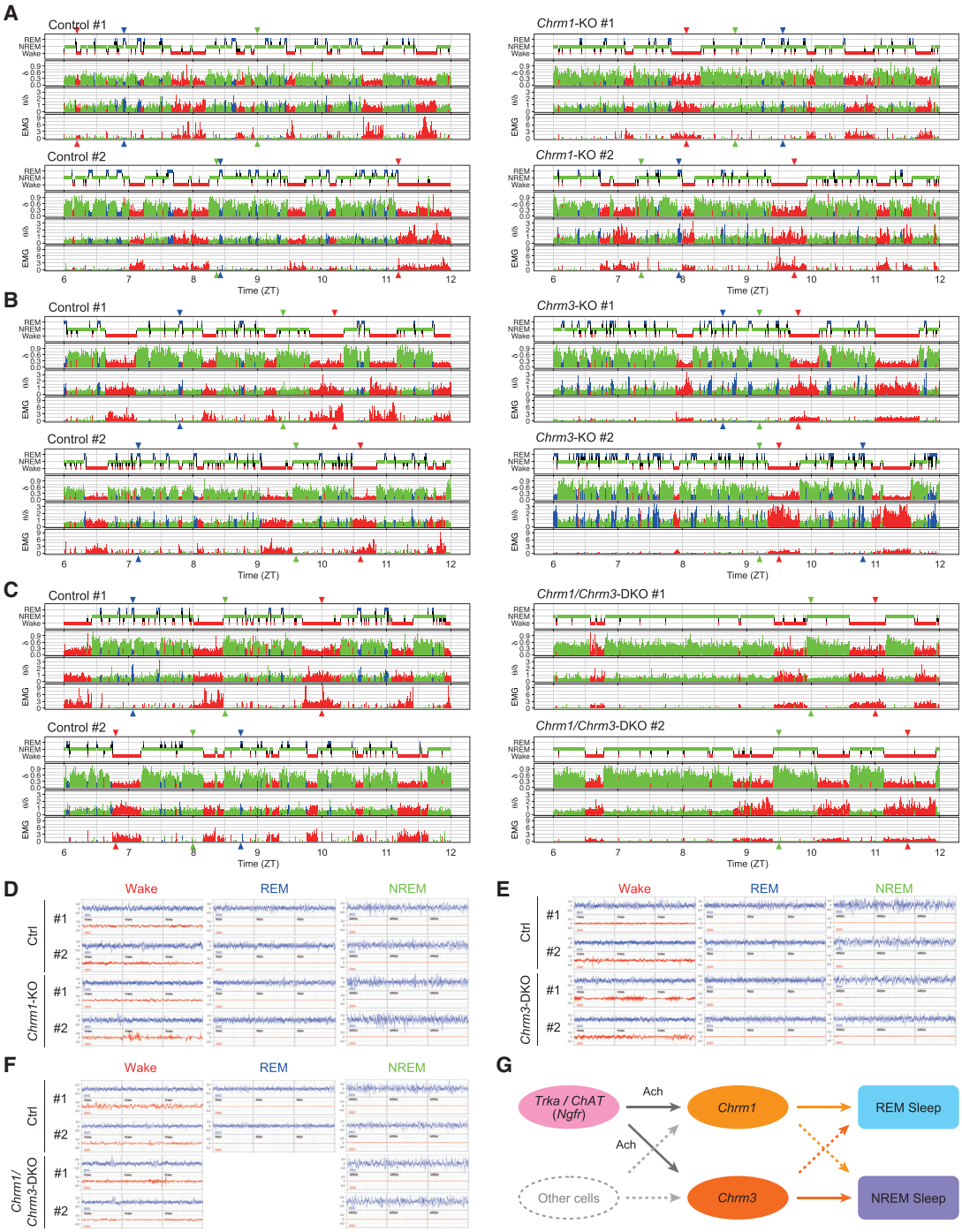

Figure 7. Detailed EEG and EMG Analysis of *Chrm1*/3 Mutants and a Schematic Representation of Ach-*Chrm1/3* Regulation of Sleep

(A–C) Hypnogram, delta power (normalized mV^2), ratio of theta/delta power, and total power of EMG wave. Two individual mice from each of *Chrm1* KO (A), *Chrm3* KO (B), *Chrm1*/*Chrm3* CRISPR DKO (C), and their control mice group were presented over ZT6–12 of the first day of EEG and EMG recording. Colored triangles indicate the arbitrary chosen position of epochs shown in (D)–(F). Red for wake, blue for REM, and green for NREM are shown.

(D–F) Representative EEG and EMG plot of two individual mice from *Chrm1* KO (D), *Chrm3* KO (E), *Chrm1*/*Chrm3* CRISPR DKO (F), and their control group. The horizontal axis represents a time of three epochs (24 s). The annotated stage (wake, NREM, or REM) is displayed for each epoch. The vertical axis represents recorded signal (in range from −0.2 to 0.2 mV) of EEG (blue) and EMG (red).

(G) A hypothetical molecular and cellular scheme for REM sleep and NREM sleep regulation. The solid line represents interaction confirmed in this study. The dashed line in a faint color means a potential interaction to be investigated in a future study. Other cells represent cholinergic sources other than *TrkA*/*ChAT*-positive cells focused in this study, such as the laterodorsal tegmentum (LDT) and the pedunculopontine tegmentum (PPT) in the brainstem.

SUPPLEMENTAL INFORMATION

Supplemental Information includes seven figures and three tables and can be found with this article online at https://doi.org/10.1016/j.celrep.2018.07.082.

ACKNOWLEDGMENTS

We thank S. Nakanishi for tetO-*EGFP*/*TeNT* mice (obtained from RIKEN BRC no. RBRC02958); D.R. Weaver for *Per1/2* DKO mice; T. Tsuji, K. Toyoshima, and K. Asakawa for FISH imaging; T. Mikami for SSS; R. Kageyama for BAC constructions; S. Yoshiura for critical comments; and I. Nikaido for administration of the server of Brainstars. We also thank all the lab members at RIKEN Center for Development Biology (CDB), QBiC, Center for Biosystems Dynamics Research (BDR), and the University of Tokyo; in particular, S. Fujino, Y. Fujiwara, K. Furuno, J. Hara, S. Hasegawa, T. Haze, N. Hori, A. Kishimoto, K. Kuwana, N. Koide, C. Kominami, M. Kunimi, K. Masawaki, E. Matsushita, A. Millius, A. Nishiyama, M. Nomura, Y. Sakakida, G. Sato, M. Shiokawa, E.A. Susaki, K. Tanaka, K. Tsujino, Y. Uranyu, M. Yamamoto, J. Yoshida-Garçon, H. Yukinaga, and Y. Wada for their kind help in preparing the materials and supporting experiments and the LARGE, RIKEN BDR for housing the mice. This work was supported by a grant from Japan Agency for Medical Research and Development (AMED)-Core Research for Evolution Science and Technology (CREST) (JP17gm0610006; AMED/Ministry of Education, Culture, Sports, Science and Technology [MEXT]; H.R.U.), CREST (Japan Science and Technology Agency [JST]/MEXT; H.R.U.), Brain Mapping by Integrated Neurotechnologies for Disease Studies (Brain/MINDS) (AMED/MEXT; H.R.U.), Basic Science and Platform Technology Program for Innovative Biological Medicine (AMED/MEXT; H.R.U.), a Grant-in-Aid for Scientific Research (S; Japan Society for the Promotion of Science [JSPS] KAKENHI grant number 25221004; H.R.U.), a Grant-in-Aid for Scientific Research (B; JSPS KAKENHI grant number 15H04408; K.S.), a Grant-in-Aid for Scientific Research on Innovative Areas (JSPS KAKENHI grant number 23115006 to H.R.U.; 26113720 to K.S.), the strategic programs for R&D (President's Discretionary Fund) of RIKEN (to H.R.U.), an intramural Grant-in-Aid from the RIKEN Quantitative Biology Center (to H.R.U.), an incentive research fund from RIKEN (to Y.N.), a Grant-in-Aid for Challenging Exploratory Research (grant number 25560427; Y.N.), a Grant-in-Aid for JSPS Fellows (grant number 13J01565; G.N.K.), a Grant-in-Aid for Young Scientists (B; grant number 16K21619; G.N.K.), the RIKEN Special Postdoctoral Research Program (to Y.N. and G.N.K.), and an ECARD grant from Queensland University of Technology (to D.P.).

AUTHOR CONTRIBUTIONS

H.R.U., Y.N., G.N.K., and R.G.Y. designed the study. K.M., M.N., T.K., and Y.S. performed microarray. M.U.-T., H.F., and K.S. performed the triple-target CRISPR. Y.N., H.U., and H.K. established genetically modified mice. Y.N., G.N.K., R.G.Y., S.S., G.A.S., and N.M. performed the sleep phenotype analysis. Y.N. and G.N.K. performed *in situ* hybridization. Y.N., G.N.K., J.G., and D.P. performed CUBIC analysis. R.G.Y., Y.N., G.N.K., and H.R.U. wrote the manuscript. All authors discussed the results and commented on the manuscript text.

DECLARATION OF INTERESTS

The authors declare no competing interests.

Received: March 14, 2018
Revised: June 3, 2018
Accepted: July 25, 2018
Published: August 28, 2018

REFERENCES

Abe, T., Sakaue-Sawano, A., Kiyonari, H., Shioi, G., Inoue, K., Horiuchi, T., Nakao, K., Miyawaki, A., Aizawa, S., and Fujimori, T. (2013). Visualization of cell cycle in mouse embryos with Fucci2 reporter directed by Rosa26 promoter. Development *140*, 237–246.

Aserinsky, E., and Kleitman, N. (1953). Regularly occurring periods of eye motility, and concomitant phenomena, during sleep. Science *118*, 273–274.

Azzalini, A., and Menardi, G. (2014). Clustering via nonparametric density estimation: the R package pdfCluster. J. Stat. Softw. *57*, 1–26.

Azzalini, A., and Torelli, N. (2007). Clustering via nonparametric density estimation. Stat. Comput. *17*, 71–80.

Bae, K., Jin, X., Maywood, E.S., Hastings, M.H., Reppert, S.M., and Weaver, D.R. (2001). Differential functions of mPer1, mPer2, and mPer3 in the SCN circadian clock. Neuron *30*, 525–536.

Basile, A.S., Fedorova, I., Zapata, A., Liu, X., Shippenberg, T., Duttaroy, A., Yamada, M., and Wess, J. (2002). Deletion of the M5 muscarinic acetylcholine receptor attenuates morphine reinforcement and withdrawal but not morphine analgesia. Proc. Natl. Acad. Sci. USA *99*, 11452–11457.

Borbély, A.A. (1982). A two process model of sleep regulation. Hum. Neurobiol. *1*, 195–204.

Brown, R.E., Basheer, R., McKenna, J.T., Strecker, R.E., and McCarley, R.W. (2012). Control of sleep and wakefulness. Physiol. Rev. *92*, 1087–1187.

Buckley, N.J., Bonner, T.I., and Brann, M.R. (1988). Localization of a family of muscarinic receptor mRNAs in rat brain. J. Neurosci. *8*, 4646–4652.

Chen, L., Yin, D., Wang, T.X., Guo, W., Dong, H., Xu, Q., Luo, Y.J., Cherasse, Y., Lazarus, M., Qiu, Z.L., et al. (2016). Basal forebrain cholinergic neurons primarily contribute to inhibition of electroencephalogram delta activity, rather than inducing behavioral wakefulness in mice. Neuropsychopharmacology *41*, 2133–2146.

Cho, S.W., Kim, S., Kim, J.M., and Kim, J.S. (2013). Targeted genome engineering in human cells with the Cas9 RNA-guided endonuclease. Nat. Biotechnol. *31*, 230–232.

Chung, S., Weber, F., Zhong, P., Tan, C.L., Nguyen, T.N., Beier, K.T., Hörmann, N., Chang, W.C., Zhang, Z., Do, J.P., et al. (2017). Identification of

preoptic sleep neurons using retrograde labelling and gene profiling. Nature *545*, 477–481.

Cong, L., Ran, F.A., Cox, D., Lin, S., Barretto, R., Habib, N., Hsu, P.D., Wu, X., Jiang, W., Marraffini, L.A., and Zhang, F. (2013). Multiplex genome engineering using CRISPR/Cas systems. Science *339*, 819–823.

Cordeau, J.P., Moreau, A., Beaulnes, A., and Laurin, C. (1963). EEG and behavioral changes following microinjections of acetylcholine and adrenaline in the brain stem of cats. Arch. Ital. Biol. *101*, 30–47.

Crick, F., and Mitchison, G. (1983). The function of dream sleep. Nature *304*, 111–114.

Dale, H. (1937). Transmission of nervous effects by acetylcholine: Harvey lecture, May 20, 1937. Bull. N. Y. Acad. Med. *13*, 379–396.

Dement, W., and Kleitman, N. (1957). Cyclic variations in EEG during sleep and their relation to eye movements, body motility, and dreaming. Electroencephalogr. Clin. Neurophysiol. *9*, 673–690.

Dement, W., Henry, P., Cohen, H., and Ferguson, J. (1967). Studies on the effect of REM deprivation in humans and in animals. Res. Publ. Assoc. Res. Nerv. Ment. Dis. *45*, 456–468.

Economo, C.V. (1930). Sleep as a problem of localization. J. Nerv. Ment. Dis. *71*, 249–259.

Freundlieb, S., Schirra-Müller, C., and Bujard, H. (1999). A tetracycline controlled activation/repression system with increased potential for gene transfer into mammalian cells. J. Gene Med. *1*, 4–12.

Funato, H., Sato, M., Sinton, C.M., Gautron, L., Williams, S.C., Skach, A., Elmquist, J.K., Skoultchi, A.I., and Yanagisawa, M. (2010). Loss of Goosecoid-like and DiGeorge syndrome critical region 14 in interpeduncular nucleus results in altered regulation of rapid eye movement sleep. Proc. Natl. Acad. Sci. USA *107*, 18155–18160.

George, R., Haslett, W.L., and Jenden, D.J. (1964). A cholinergic mechanism in the brainstem reticular formation: induction of paradoxical sleep. Int. J. Neuropharmacol. *3*, 541–552.

Gotti, C., and Clementi, F. (2004). Neuronal nicotinic receptors: from structure to pathology. Prog. Neurobiol. *74*, 363–396.

Goutagny, R., Comte, J.C., Salvert, D., Gomeza, J., Yamada, M., Wess, J., Luppi, P.H., and Fort, P. (2005). Paradoxical sleep in mice lacking M3 and M2/M4 muscarinic receptors. Neuropsychobiology *52*, 140–146.

Hayashi, Y., Kashiwagi, M., Yasuda, K., Ando, R., Kanuka, M., Sakai, K., and Itohara, S. (2015). Cells of a common developmental origin regulate REM/non-REM sleep and wakefulness in mice. Science *350*, 957–961.

Hayes, M.H. (1996). Statistical Digital Signal Processing and Modeling (John Wiley & Sons).

Hobson, J.A., McCarley, R.W., and Wyzinski, P.W. (1975). Sleep cycle oscillation: reciprocal discharge by two brainstem neuronal groups. Science *189*, 55–58.

Holtzman, D.M., Kilbridge, J., Li, Y., Cunningham, E.T., Jr., Lenn, N.J., Clary, D.O., Reichardt, L.F., and Mobley, W.C. (1995). TrkA expression in the CNS: evidence for the existence of several novel NGF-responsive CNS neurons. J. Neurosci. *15*, 1567–1576.

Imayoshi, I., Ohtsuka, T., Metzger, D., Chambon, P., and Kageyama, R. (2006). Temporal regulation of Cre recombinase activity in neural stem cells. Genesis *44*, 233–238.

Jouvet, M. (1962). [Research on the neural structures and responsible mechanisms in different phases of physiological sleep]. Arch. Ital. Biol. *100*, 125–206.

Kamsler, A., McHugh, T.J., Gerber, D., Huang, S.Y., and Tonegawa, S. (2010). Presynaptic m1 muscarinic receptors are necessary for mGluR long-term depression in the hippocampus. Proc. Natl. Acad. Sci. USA *107*, 1618–1623.

Kasukawa, T., Masumoto, K.H., Nikaido, I., Nagano, M., Uno, K.D., Tsujino, K., Hanashima, C., Shigeyoshi, Y., and Ueda, H.R. (2011). Quantitative expression profile of distinct functional regions in the adult mouse brain. PLoS ONE *6*, e23228.

Kodama, T., Takahashi, Y., and Honda, Y. (1990). Enhancement of acetylcholine release during paradoxical sleep in the dorsal tegmental field of the cat brain stem. Neurosci. Lett. *114*, 277–282.

Krenzer, M., Anaclet, C., Vetrivelan, R., Wang, N., Vong, L., Lowell, B.B., Fuller, P.M., and Lu, J. (2011). Brainstem and spinal cord circuitry regulating REM sleep and muscle atonia. PLoS ONE *6*, e24998.

Lee, T., and Luo, L. (1999). Mosaic analysis with a repressible cell marker for studies of gene function in neuronal morphogenesis. Neuron *22*, 451–461.

Lein, E.S., Hawrylycz, M.J., Ao, N., Ayres, M., Bensinger, A., Bernard, A., Boe, A.F., Boguski, M.S., Brockway, K.S., Byrnes, E.J., et al. (2007). Genome-wide atlas of gene expression in the adult mouse brain. Nature *445*, 168–176.

Li, L., Tasic, B., Micheva, K.D., Ivanov, V.M., Spletter, M.L., Smith, S.J., and Luo, L. (2010). Visualizing the distribution of synapses from individual neurons in the mouse brain. PLoS ONE *5*, e11503.

Li, W., Ma, L., Yang, G., and Gan, W.B. (2017). REM sleep selectively prunes and maintains new synapses in development and learning. Nat. Neurosci. *20*, 427–437.

Lu, J., Sherman, D., Devor, M., and Saper, C.B. (2006). A putative flip-flop switch for control of REM sleep. Nature *441*, 589–594.

Ma, M., Ye, A.Y., Zheng, W., and Kong, L. (2013). A guide RNA sequence design platform for the CRISPR/Cas9 system for model organism genomes. BioMed Res. Int. *2013*, 270805.

McCarley, R.W. (2004). Mechanisms and models of REM sleep control. Arch. Ital. Biol. *142*, 429–467.

McGinty, D.J., and Sterman, M.B. (1968). Sleep suppression after basal forebrain lesions in the cat. Science *160*, 1253–1255.

Mizushima, S., and Nagata, S. (1990). pEF-BOS, a powerful mammalian expression vector. Nucleic Acids Res. *18*, 5322.

Nauta, W.J. (1946). Hypothalamic regulation of sleep in rats; an experimental study. J. Neurophysiol. *9*, 285–316.

Ode, K.L., Katsumata, T., Tone, D., and Ueda, H.R. (2017a). Fast and slow Ca^{2+}-dependent hyperpolarization mechanisms connect membrane potential and sleep homeostasis. Curr. Opin. Neurobiol. *44*, 212–221.

Ode, K.L., Ukai, H., Susaki, E.A., Narumi, R., Matsumoto, K., Hara, J., Koide, N., Abe, T., Kanemaki, M.T., Kiyonari, H., and Ueda, H.R. (2017b). Knockout-rescue embryonic stem cell-derived mouse reveals circadian-period control by quality and quantity of CRY1. Mol. Cell *65*, 176–190.

Preibisch, S., Saalfeld, S., and Tomancak, P. (2009). Globally optimal stitching of tiled 3D microscopic image acquisitions. Bioinformatics *25*, 1463–1465.

R Development Core Team (2016). R: A language and environment for statistical computing (R Foundation for Statistical Computing).

Ramos, O.V., Torterolo, P., Lim, V., Chase, M.H., Sampogna, S., and Yamuy, J. (2011). The role of mesopontine NGF in sleep and wakefulness. Brain Res. *1413*, 9–23.

Ran, F.A., Hsu, P.D., Wright, J., Agarwala, V., Scott, D.A., and Zhang, F. (2013). Genome engineering using the CRISPR-Cas9 system. Nat. Protoc. *8*, 2281–2308.

Reijmers, L.G., Perkins, B.L., Matsuo, N., and Mayford, M. (2007). Localization of a stable neural correlate of associative memory. Science *317*, 1230–1233.

Sato, H., Amagai, K., Shimizukawa, R., and Tamai, Y. (2009). Stable generation of serum- and feeder-free embryonic stem cell-derived mice with full germline-competency by using a GSK3 specific inhibitor. Genesis *47*, 414–422.

Schindelin, J., Arganda-Carreras, I., Frise, E., Kaynig, V., Longair, M., Pietzsch, T., Preibisch, S., Rueden, C., Saalfeld, S., Schmid, B., et al. (2012). Fiji: an open-source platform for biological-image analysis. Nat. Methods *9*, 676–682.

Shi, M., Yue, Z., Kuryatov, A., Lindstrom, J.M., and Sehgal, A. (2014). Identification of Redeye, a new sleep-regulating protein whose expression is modulated by sleep amount. eLife *3*, e01473.

Shi, Y.F., Han, Y., Su, Y.T., Yang, J.H., and Yu, Y.Q. (2015). Silencing of cholinergic basal forebrain neurons using archaerhodopsin prolongs slow-wave sleep in mice. PLoS ONE *10*, e0130130.

Sobreviela, T., Clary, D.O., Reichardt, L.F., Brandabur, M.M., Kordower, J.H., and Mufson, E.J. (1994). TrkA-immunoreactive profiles in the central nervous system: colocalization with neurons containing p75 nerve growth factor receptor, choline acetyltransferase, and serotonin. J. Comp. Neurol. *350*, 587–611.

Sumiyama, K., Kawakami, K., and Yagita, K. (2010). A simple and highly efficient transgenesis method in mice with the Tol2 transposon system and cytoplasmic microinjection. Genomics *95*, 306–311.

Sunagawa, G.A., Séi, H., Shimba, S., Urade, Y., and Ueda, H.R. (2013). FASTER: an unsupervised fully automated sleep staging method for mice. Genes Cells *18*, 502–518.

Sunagawa, G.A., Sumiyama, K., Ukai-Tadenuma, M., Perrin, D., Fujishima, H., Ukai, H., Nishimura, O., Shi, S., Ohno, R.I., Narumi, R., et al. (2016). Mammalian reverse genetics without crossing reveals Nr3a as a short-sleeper gene. Cell Rep. *14*, 662–677.

Susaki, E.A., Tainaka, K., Perrin, D., Kishino, F., Tawara, T., Watanabe, T.M., Yokoyama, C., Onoe, H., Eguchi, M., Yamaguchi, S., et al. (2014). Whole-brain imaging with single-cell resolution using chemical cocktails and computational analysis. Cell *157*, 726–739.

Susaki, E.A., Tainaka, K., Perrin, D., Yukinaga, H., Kuno, A., and Ueda, H.R. (2015). Advanced CUBIC protocols for whole-brain and whole-body clearing and imaging. Nat. Protoc. *10*, 1709–1727.

Tainaka, K., Kubota, S.I., Suyama, T.Q., Susaki, E.A., Perrin, D., Ukai-Tadenuma, M., Ukai, H., and Ueda, H.R. (2014). Whole-body imaging with single-cell resolution by tissue decolorization. Cell *159*, 911–924.

Tatsuki, F., Sunagawa, G.A., Shi, S., Susaki, E.A., Yukinaga, H., Perrin, D., Sumiyama, K., Ukai-Tadenuma, M., Fujishima, H., Ohno, R., et al. (2016). Involvement of Ca(2+)-dependent hyperpolarization in sleep duration in mammals. Neuron *90*, 70–85.

Teles-Grilo Ruivo, L.M., Baker, K.L., Conway, M.W., Kinsley, P.J., Gilmour, G., Phillips, K.G., Isaac, J.T.R., Lowry, J.P., and Mellor, J.R. (2017). Coordinated acetylcholine release in prefrontal cortex and hippocampus is associated with arousal and reward on distinct timescales. Cell Rep. *18*, 905–917.

Tsujino, K., Narumi, R., Masumoto, K.H., Susaki, E.A., Shinohara, Y., Abe, T., Iigo, M., Wada, A., Nagano, M., Shigeyoshi, Y., and Ueda, H.R. (2013). Establishment of TSH β real-time monitoring system in mammalian photoperiodism. Genes Cells *18*, 575–588.

Ukai, H., Kiyonari, H., and Ueda, H.R. (2017). Production of knock-in mice in a single generation from embryonic stem cells. Nat. Protoc. *12*, 2513–2530.

Wada, N., Kishimoto, Y., Watanabe, D., Kano, M., Hirano, T., Funabiki, K., and Nakanishi, S. (2007). Conditioned eyeblink learning is formed and stored without cerebellar granule cell transmission. Proc. Natl. Acad. Sci. USA *104*, 16690–16695.

Wang, H., Yang, H., Shivalila, C.S., Dawlaty, M.M., Cheng, A.W., Zhang, F., and Jaenisch, R. (2013). One-step generation of mice carrying mutations in multiple genes by CRISPR/Cas-mediated genome engineering. Cell *153*, 910–918.

Warming, S., Costantino, N., Court, D.L., Jenkins, N.A., and Copeland, N.G. (2005). Simple and highly efficient BAC recombineering using galK selection. Nucleic Acids Res. *33*, e36.

Weber, F., and Dan, Y. (2016). Circuit-based interrogation of sleep control. Nature *538*, 51–59.

Weng, F.J., Williams, R.H., Hawryluk, J.M., Lu, J., Scammell, T.E., Saper, C.B., and Arrigoni, E. (2014). Carbachol excites sublaterodorsal nucleus neurons projecting to the spinal cord. J. Physiol. *592*, 1601–1617.

Wess, J. (2004). Muscarinic acetylcholine receptor knockout mice: novel phenotypes and clinical implications. Annu. Rev. Pharmacol. Toxicol. *44*, 423–450.

Xiao, Z., Deng, P.Y., Yang, C., and Lei, S. (2009). Modulation of GABAergic transmission by muscarinic receptors in the entorhinal cortex of juvenile rats. J. Neurophysiol. *102*, 659–669.

Xu, W., Gelber, S., Orr-Urtreger, A., Armstrong, D., Lewis, R.A., Ou, C.N., Patrick, J., Role, L., De Biasi, M., and Beaudet, A.L. (1999). Megacystis, mydriasis, and ion channel defect in mice lacking the alpha3 neuronal nicotinic acetylcholine receptor. Proc. Natl. Acad. Sci. USA *96*, 5746–5751.

Xu, M., Chung, S., Zhang, S., Zhong, P., Ma, C., Chang, W.C., Weissbourd, B., Sakai, N., Luo, L., Nishino, S., and Dan, Y. (2015). Basal forebrain circuit for sleep-wake control. Nat. Neurosci. *18*, 1641–1647.

Yamamoto, M., Wada, N., Kitabatake, Y., Watanabe, D., Anzai, M., Yokoyama, M., Teranishi, Y., and Nakanishi, S. (2003). Reversible suppression of glutamatergic neurotransmission of cerebellar granule cells in vivo by genetically manipulated expression of tetanus neurotoxin light chain. J. Neurosci. *23*, 6759–6767.

Yasuda, R.P., Ciesla, W., Flores, L.R., Wall, S.J., Li, M., Satkus, S.A., Weisstein, J.S., Spagnola, B.V., and Wolfe, B.B. (1993). Development of antisera selective for m4 and m5 muscarinic cholinergic receptors: distribution of m4 and m5 receptors in rat brain. Mol. Pharmacol. *43*, 149–157.

Zant, J.C., Kim, T., Prokai, L., Szarka, S., McNally, J., McKenna, J.T., Shukla, C., Yang, C., Kalinchuk, A.V., McCarley, R.W., et al. (2016). Cholinergic neurons in the basal forebrain promote wakefulness by actions on neighboring non-cholinergic neurons: an opto-dialysis study. J. Neurosci. *36*, 2057–2067.

STAR★METHODS

KEY RESOURCES TABLE

REAGENT or RESOURCE	SOURCE	IDENTIFIER
Antibodies		
anti-Dig-Fab-AP	Merck	Cat# 11093274910; RRID: AB_2734716
Anti-Fluorescein-HRP	PerkinElmer	Cat# NEF710001EA
Anti-Digoxigenin-POD, Fab fragments from sheep	Roche	Cat# 11207733910; RRID: AB_514500
Deposited Data		
Expression profile of adult mouse BF and/or POA regions	This paper	GEO: GSE107500
Experimental Models: Cell Lines		
Human: HEK293T	ATCC	CRL-3216
Experimental Models: Organisms/Strains		
Mouse:Tg(tetO-tdTomato,-Syp/EGFP*)1.1Luo/Jz	The Jackson Laboratory	JAX: 012345
Mouse:B6;DBA-Tg(Fos-tTA,Fos-EGFP*)1Mmay Tg(tetO-lacZ,tTA*)1Mmay/J	The Jackson Laboratory	JAX:008344
Mouse:C57BL/6J-Tg(tetO-EGFP/TeNT)1Nak	RIKEN BRC	RBRC02958
Mouse: TrkA-tTA	This paper	N/A
Mouse: Ngfr-tTA	This paper	N/A
Mouse: ChAT-tTR-nmNGx3	This paper	N/A
Mouse: VGluT1-tTR-nmNGx3	This paper	N/A
Oligonucleotides		
Oligonucleotides for FISH, see Table S1	This paper	N/A
Oligonucleotides for triple-target CRISPR, see Table S2	This paper	N/A
Oligonucleotides for plasmid DNA construction, see STAR methods	This paper	N/A
Recombinant DNA		
pEF-BOS	Mizushima and Nagata, 1990	N/A
pRL-SV40	Promega	N/A

CONTACT FOR REAGENT AND RESOURCE SHARING

Further information and requests for reagents should be directed to Lead Contact Hiroki R. Ueda (uedah-tky@umin.ac.jp).

EXPERIMENTAL MODEL AND SUBJECT DETAILS

Cultivation of mouse embryonic stem (ES) cells

Cultivation of mouse ES cells was conducted with the same protocol described in the previous report (Ode et al., 2017b; Ukai et al., 2017). Before cultivation, the surface of PURECoat^{TM} amine dishes (Beckton-Dickinson, NJ, U.S.A.) were exposed to medium containing LIF plus 6-bromoindirubin-30-oxime (BIO) (Sato et al., 2009) for more than 5 hours at 37°C with 5% CO_2. ES cells were cultured with or without feeder cells in 3i medium (Clontech Laboratories, Inc. A Takara Bio Company, Japan) at 37°C with 5% CO_2.

Mice and sleep phenotyping

All experimental procedures and housing conditions were approved by the Institutional Animal Care and Use Committee of RIKEN Kobe Branch, and all the animals were cared for and treated humanely in accordance with the Institutional Guidelines for Experiments using Animals. All mice were given food and water *ad libitum* and maintained at ambient temperature and humidity. The light was controlled under 12 h light and 12 h dark cycle. Production and sleep phenotyping of *Chrna2*, *Chrna4, Chrna5, Chrna6, Chrna7, Chrna9, Chrna10, Chrnb2,* and *Chrnb4* KO mice were performed in RIKEN CDB at Kobe using the sleep phenotype of C57BL/6N mice (n = 108) published in our previous paper for data on control mice (Sunagawa et al., 2016). Creation and sleep phenotyping of *Chrnb3*, *Chrm1, Chem2, Chrm3, Chrm4,* and *Chrm5* KO mice were performed in RIKEN QBiC at Osaka using C57BL/6N mice (n = 107) for control data.

Transfection and Luciferase Assay

293T cells (American Type Culture Collection, ATCC) were maintained in DMEM (Thermo Fisher Scientific, MA, U.S.A.) supplemented with 10% FBS (Merck, Germany) and antibiotics (100 U/mL penicillin and 100 μg/mL streptomycin; Thermo Fisher Scientific, MA, U.S.A.) at 37°C with 5% CO_2. One day prior to transfection, cells were plated onto 35 mm dishes at a density of 4×10^5 cells per well. The following day, 293T cells were co-transfected using FuGene6 (Roche, Switzerland) with 0.2 μg of a luciferase reporter plasmid (ptetO-Luc) and the indicated amount (μg) of effector plasmids (pEF-tTA and pEF-tTR) (pEF-BOS vectors were previously developed (Mizushima and Nagata, 1990)) in Figure 3B (n = 3), according to the manufacturer's instructions, and cultured at 37°C. Empty vector was used to make up the total amount of DNA to 2 μg per well. Additionally, 40 ng of a pRL-SV40 plasmid (*Renilla* luciferase (RLuc) reporter vector; Promega, WI, U.S.A.) was added to each transfection as an internal control for transfection efficiency. Twenty-four hours after transfection, cells were harvested and assayed with a Dual-Luciferase Reporter Assay System (Promega, WI, U.S.A.). Luciferase (FLuc) activity was normalized by RLuc activity. Data are representative of two independent experiments.

METHOD DETAILS

Sampling of POA/BF regions

The samples of POA/BF regions were collected with the same protocol used in the previous report (Kasukawa et al., 2011). That is, 5-week BALB/c male mice were conditioned under a standard 12:12 light/dark cycle (LD) for 2 weeks, and samples were obtained under LD or constant darkness (DD) conditions every 4 h for 1 day starting at ZT0. At each time point, 0.5 mm-thick slices of mouse brain were cut on a Mouse Brain Matrix (Neuroscience Inc., Japan) and frozen. POA/BF regions in the brain slices were punched out bilaterally with a microdissecting needle (gauge 0.5 mm) under a stereomicroscope. We sampled 25 mice at each time point. The whole procedure was repeated twice (n = 2) to obtain experimental replicates.

Microarray analysis

In obtaining an expression profile of POA/BF regions, we used the same experimental procedure as one used in the previous report (Kasukawa et al., 2011). Briefly, total RNA was extracted from the pooled POA/BF samples using Trizol reagent (Thermo Fisher Scientific, MA, U.S.A.). RNA samples were reverse transcribed, labeled, and hybridized to Affymetrix GeneChip Mouse Genome 430 2.0 according to the manufacturer's instruction (Affymetrix one-cycle method). The expression values were summarized together with the samples used in the previous report (Kasukawa et al., 2011) by the RMA method. CNS region-specific genes were identified with the method described in the previous report (GEO; GSE107500) (Kasukawa et al., 2011).

Generation of TrkA-tTA and Ngfr-tTA transgenic mouse lines

BAC DNAs (R24-222B4 for *TrkA-tTA* and R24-309N6 for *Ngfr-tTA*) were obtained from BACPAC resources center at CHORI. BAC modification was performed by recombineering (Warming et al., 2005). Briefly, *tTA* and *SV40* polyA signal sequences were amplified from pTet-off (Clontech, CA, U.S.A.) and inserted into just after the start codon of *TrkA* or *Ngfr* genes by recombineering. Modified BAC DNAs were confirmed by electrophoresis and purified by NucleoBond Xtra midi (Macherey-Nagel, Germany). Purified transgene DNA was eluted with TE (10 mM Tris, 1 mM EDTA, pH 8.0) buffer, diluted with PBS(-) buffer to a final concentration of 5 ng/μL, and injected into pronuclei of C57BL/6N zygotes as reported previously (Abe et al., 2013). Transgenic lines termed *TrkA-tTA* (Accession number CDB0522T: http://www2.clst.riken.jp/arg/TG%20mutant%20mice%20list.html) and *Ngfr-tTA* (Accession number CDB0523T: http://www2.clst.riken.jp/arg/TG%20mutant%20mice%20list.html) were selected for analysis based on PCR screening and fertility. Transgenic lines were successively backcrossed with C57BL/6N; mice were genotyped by PCR with the primers 5′-ggaaggcgagctggcattagggcctcaaaa-3′, 5′-cgacatccagacagtgactgcgcggctctg-3′, and 5′-tcttgccatgactcgccttccaggggcag-3′ for *TrkA-tTA*, and the primers 5′-gaggaggcggggctgctgcattgccttcac-3′, 5′-gactgctcccagtctcctacaccgcacccg-3′, and 5′-tcttgccat gactcgccttccaggggcag-3′ for *Ngfr-tTA*, yielding 619 bp and 434 bp products (*TrkA-tTA*) and 585 bp and 426 bp products (*Ngfr-tTA*), respectively.

Construction of tTR

Our tTR system is similar to the tetracycline-controlled transcriptional silencer (tTS), which was originally developed to repress basal tetO promoter activity by blocking reverse tetracycline-controlled transactivator (rtTA) in the absence of doxycyline (dox) (Freundlieb et al., 1999). tTS doesn't bind to rtTA because it is not intended to interrupt rtTA's induction activity in the presence of dox. *tTR* was designed and generated by replacing the transcription activator domain of *tTA* with NLS and KRAB transcription suppressor domains (underlined in the following sequence) so that it could form a tTA-tTR heterodimer and effectively repress tTA activity. The amino acid sequence of tTR is as follows:

MSRLDKSKVINSALELLNEVGIEGLTTRKLAQKLGVEQPTLYWHVKNKRALLDALAIEMLDRHHTHFCPLEGESWQDFLRNNAKSFRC ALLSHRDGAKVHLGTRPTEKQYETLENQLAFLCQQGFSLENALYALSAVGHFTLGCVLEDQEHQVAKEERETPTTDSMPPLLRQAIELFD HQGAEPAFLFGLELIICGLEKQLKCESGGPKKKRKLAVSVTFEDVAVLFTRDEWKKLDLSQRSLYREVMLENYSNLASMAGFLFTKPKVI SLLQQGEDPW*

Generation of ChAT-tTR-nmNGx3 and VGluT1-tTR-nmNGx3 KI mice

tTR fused with P2A at the N terminus, T2A at the C terminus, and BGH polyA were synthesized and cloned into the pENTR vector (ThermoFisher, USA) to make pENTR-2A-tTR. mNeonGreen (Allele Biotechnology, U.S.A.) with an NLS at the N terminus and two mNeonGreen were amplified and fused tandemly into nmNGx3. Then, nmNGx3 was cloned into the EcoRI site of the pENTR-2A-tTR vector by ligation. Destination vectors for targeting into the C terminus of the cholinergic marker gene *choline acetyltransferase (ChAT)* and the glutamatergic marker gene *vesicular glutamate transporter 1* (*VGluT1)* were constructed as follows:

Right-homology arms were amplified by PCR with the primers listed: forward primer for *ChAT* (5′-ggctcgatccctcgagttgggggctca catgaagctgg-3′), reverse primer for *ChAT* (5′-cgggaattcgatgatatcgaatgcatcactgcttcaaacaactgtc-3′), forward primer for *VGluT1* (5′-ggctcgatccctcgaggcctgagcggcagtgtcgagg-3′), and reverse primer for *VGluT1* (5′-cgggaattcgatgatatcgagcagagaaactgaggtgca gac-3′). The PCR products were inserted into the *Xho*I and *Eco*RV digested back-bone vector pTVCl3 (Tainaka et al., 2014) using the In-Fusion HD Cloning Kit (Clontech Laboratories, Inc. A Takara Bio Company, Japan). Left-homology arms were amplified by PCR with primers as listed: forward primer for *ChAT* (5′-tagggataacagggtaatatagaggtgacagcaggattggaagtg-3′), reverse primer for *ChAT* (5′-gcggagaaagaggtaatgaaatgggcgtgggagtagtcaagattgcttgg-3′), forward primer for *VGluT1* (5′-tagggataacagggtaata tagccctcgctatgccagcatcttg-3′), and reverse primer for *VGluT1* (5′-gcggagaaagaggtaatgaaatgggcgtagtcccggacaggggcg-3′). The products of first PCR for the left-homology arms were amplified with primers (5′-gcagttacgctagggataacagggtaatatag-3′ and 5′-gat catctatgtcgggtgcggagaaagaggtaatgaaatgg-3′) and inserted into the I-SceI and PI-SceI digested pTVCl3-Rarm using the In-Fusion HD Cloning Kit. The puromycin resistance gene cassette (P(PGK)-Puro^R-polyA) was inserted into I-CeuI and PI-PspI digested pTVCl3-LRarm.

Targeting, screening, and injection were performed according to the procedures described previously (Ode et al., 2017b; Ukai et al., 2017).

Triple-target CRISPR: gRNA synthesis

The target sequences for *Chrna2*, *Chrna4, Chrna5, Chrna6, Chrna7, Chrna9, Chrna10, Chrnb2, Chrnb3, Chrnb4* (Figures S5A–S5J), *Chrm1* (set 1 and 2), *Chrm2, Chrm3* (set 1 and 2), *Chrm4,* and *Chrm5* (Figures S6A–S6E, S6K, and S6L) were designed using the on-line CRISPR guide RNA Design tool (Ma et al., 2013) or the mm10 CRISPR/Cas9 database (Sunagawa et al., 2016) (http://crispr.riken.jp/). Possible off-target sequences within the mouse genome for each target sequence were checked using the CRISPR Design Tool (Ran et al., 2013) (http://tools.genome-engineering.org).

Guide RNA (gRNA) synthesis was performed using the same protocol described in the previous report (Sunagawa et al., 2016). The gRNA templates were directly synthesized and fused to the T7 promoter by PCR. First, partial fragments of the gRNA templates including each target sequence were amplified from the pX330 plasmids (Addgene, #42230) (Cong et al., 2013; Ran et al., 2013) by PCR with the common reverse primer (5′-aaaagcaccgactcggtgcc-3′; Hokkaido System Science, Japan or Fasmac, Japan) (Wang et al., 2013) and forward primer-1 for each target sequence (Table S2A, Hokkaido System Science, or Fasmac). Subsequently, the T7 promoter-fused gRNA templates were amplified from the diluted PCR products by PCR with the common reverse primer and forward primer-2 for each target sequence (Table S2A, Hokkaido System Science, or Fasmac). The T7 promoter-fused gRNA PCR fragments were used as a template for *in vitro* transcription using the MEGAshortscript T7 kit (Thermo Fisher Scientific, MA, U.S.A.). The gRNAs were purified using the MEGAclear kit (Thermo Fisher Scientific, MA, U.S.A.).

Triple-target CRISPR: Cas9 mRNA synthesis

Cas9 mRNAs were synthesized with the same protocol described in the previous report (Sunagawa et al., 2016). The p3s-Cas9HC plasmid (Cho et al., 2013) (Addgene, #43945), which includes a T7 promoter-fused *Cas9* coding region, was digested with XbaI (Takara Bio Inc., Japan), and used as the template for *in vitro* transcription using the mMESSAGE mMACHINE T7 kit (Thermo Fisher Scientific, MA, U.S.A.). The *Cas9* mRNA was purified using the MEGAclear kit (Thermo Fisher Scientific, MA, U.S.A.).

Triple-target CRISPR: One-cell embryo microinjection

One-cell embryo microinjection was conducted by the same protocol described in the previous report (Sunagawa et al., 2016). C57BL/6N females (4–6 weeks old, CLEA Japan Inc) were superovulated and mated with C57BL/6N males (CLEA Japan Inc., Japan). Fertilized eggs were collected from the ampulla of the oviduct of plugged C57BL/6N females by micro-dissection, and maintained in KSOM medium (Merck, Germany or ARK Resource, Japan) in a 5% CO_2 incubator at 37°C. *Cas9* mRNA (100 ng/μL) and gRNAs (150 ng/μL in total) were co-injected into the cytoplasm of fertilized eggs in M2 medium (Merck Millipore or ARK Resource) at room temperature (23–25°C). Details of the cytoplasmic injection were reported previously (Sumiyama et al., 2010). After microinjection, the embryos were cultured for 1 h in KSOM medium (Merck, Germany or ARK Resource, Japan) in a 5% CO_2 incubator at 37°C, and 25–35 embryos were then transferred to the oviducts of pseudopregnant female ICR mice.

Triple-target CRISPR: Genotyping of KO mice and ESCs by quantitative PCR (qPCR) and sequencing

Genotyping of KO mice was conducted with the same protocol described in the previous report (Sunagawa et al., 2016). Genomic DNA of wild-type and KO mice was prepared from their tails using the DNeasy Blood & Tissue Kit (QIAGEN, Germany), according to the manufacturer's instructions. qPCR for genotyping was performed using the ABI PRISM 7900/QuantStudio 7 Flex (Thermo Fisher Scientific, MA, U.S.A.) and the SYBR Premix Ex Taq GC (Takara Bio Inc., Japan). Primers for qPCR (Table S2B, Hokkaido System

Science, or Fasmac) were annealed to the targeting sequences. The absolute target site abundance was calculated using a standard curve obtained from wild-type genomic DNA. The amount of *Tbp* (Tsujino et al., 2013) was quantified and used as an internal control. When we could not confirm KO genotype by qPCR, we performed sequencing or a second qPCR using alternative primers, which were independent of first qPCR.

Establishment of Chrm1/3 dKO ES cell

One-cell embryo, Cas9 mRNA, and gRNAs were prepared as described above. *Cas9* mRNA (100 ng/μL) and gRNAs (150 ng/μL in total) were co-injected into the cytoplasm of 200 fertilized eggs in M2 medium (Merck Millipore, MA, U.S.A. or ARK Resource, Japan) at room temperature (23–25°C) as described above. After microinjection, the embryos were cultured for 2 days in KSOM medium (Merck Millipore, MA, U.S.A. or ARK Resource, Japan) in a 5% CO_2 incubator at 37°C.

On the next day of injection, mitotic-inactivated MEFs were seeded into the wells of 1% gelatin-coated 4-well plates (1.5×10^5 cells/well) with mouse ES medium. The next day, ES medium was replaced with 3i medium, and the plates were incubated for at least 30 min at 37°C in 5% CO_2 before use.

Two days after injection, 50 embryos that had developed to the 8-cell stage or later were transferred into 3i-culture medium on the feeder-coated dish. Embryos were incubated at 37°C in 5% CO_2 without replacing the medium for 10 days or more, until a lump-like ES colony (primary colony) appeared.

On the day before proceeding to the next step, BIO medium-treated amine-coated wells (24-well plate), one well for each colony, were prepared. After incubation of the BIO-containing plates overnight at 37°C in 5% CO_2, BIO-medium was replaced with 3i-culture medium, and then the plates were incubated at 37°C in 5% CO_2.

After confirming proliferation of the primary colony, culture medium was replaced with fresh 3i medium (pre-warmed to 37°C) and incubation continued for 3 h at 37°C in 5% CO_2. After washing the colony with PBS(-), trypsinized cells derived from each colony were harvested, and transferred into the BIO medium-treated amine-coated well containing 3i-culture medium. After cultivation for several days at 37°C in 5% CO_2 without replacing the medium, the colonies were cloned, expanded, stored, and used for genomic DNA extraction (Ode et al., 2017b; Ukai et al., 2017).

The sex of the ES clones was determined by PCR on the *Sry* gene with the following primers: Sry-F, 5′-ccatgtcaagcgccccatga-3′; Sry-R, 5′-gtaaggcttttccacctgca-3′ (Hokkaido System Science, Japan or Fasmac, Japan). Genotyping by qPCR was performed as described above. The KO-ESC clones were injected in 8-cell-stage embryos and chimerism confirmed according to a previously reported protocol (Ode et al., 2017b; Ukai et al., 2017).

Sleep measurement with SSS

SSS recording and analysis were carried out according to the protocol described previously (Sunagawa et al., 2016). One set of data recording in the SSS chamber was for one week. During the experiment, neither the chamber nor the rack was opened except for the sleep-deprivation experiment. The light condition of the SSS rack was set to the LD (12:12 light-dark) or the DD (constant dark) condition, and food and water were given *ad libitum*. For data analysis, six days from the second recording date were used. The control dataset of C57BL/6N wild-type mice were shared among different groups of mutant mice for analysis (Table S3).

Sleep parameters, such as sleep duration, amplitude, P_{WS}, and P_{SW} were defined previously (Sunagawa et al., 2016). For the present study, the definition of transition probabilities are as follows: The P_{WS} and P_{SW} represent different probabilities in regard to the direction of wake/sleep transition. For example, when a mouse shows a long sleep phonotype, its P_{WS} (transition probability from wake to sleep) tends to be large while the P_{SW} (transition probability from wake to sleep) tends to be small. More precisely, P_{WS} is defined as $P_{WS} = N_{WS}/(N_{WS}+N_{WW})$ where N_{WS} and N_{WW} are the numbers of transition in the direction from wake to sleep and wake to wake (i.e., stay in wake), respectively, in the observed period. On the other hand, P_{SW} is defined as $N_{SW}/(N_{SW}+N_{SS})$ where N_{SW} and N_{SS} are the numbers of transition in the direction from sleep to wake and sleep to sleep (i.e., stay in sleep), respectively, in the observed period. Similarly, P_{WW} and P_{SS} can also be defined. According to these definitions, it can be noticed that $P_{SW} + P_{SS} = 1$ and $P_{WS} + P_{WW} = 1$. Therefore, P_{SW} and P_{WS} reflect, in addition to the aforementioned wake/sleep propensities, the stabilities of sleep (P_{SS}) and wake (P_{WW}), respectively (Sunagawa et al., 2016).

Sleep measurement with EEG and EMG recordings

Telemetry EEG and EMG recording devices (DSI, MN, U.S.A.) were implanted into mice more than 10 days before recording. Further information on implantation of telemetry devices been described previously (Sunagawa et al., 2013). For the sleep staging, we used the FASTER method to automatically annotate EEG and EMG data (Sunagawa et al., 2013), and then the result of the FASTER annotation was corrected by visual inspection. In the automated staging of the FASTER method, EEG and EMG data were divided into 8 s segments (epochs), and each epoch was detrended by subtracting a linear trend, which was estimated by the least-squares linear regression. The power spectrum of the epoch was obtained by FFT with the Hann window. Both data arrays of the power spectrum of EEG and EMG from the same epoch were concatenated into a single array, and then the concatenated array of spectrum data was subjected to principal component analysis. The top four principal components were used for the subsequent clustering which was performed by the *pdfCluster* library (Azzalini and Menardi, 2014; Azzalini and Torelli, 2007). To reduce computational load for

clustering, the epochs of a whole time series were divided into subsets of epochs so that each subset was comprised of 5400 epochs, and within each subset, clusters were produced. The produced clusters were annotated by the following rules: First, the median logarithm of EMG power of each cluster was computed and clusters that have higher median logarithm of EMG power than the 0.5 quartiles of that of all data points were annotated as 'Wake'. Within the remaining non-wake clusters, median logarithm of EEG delta power (0.5–4 Hz) was calculated, and if it was greater than 0.1 quartile of EEG delta power among all non-wake data points, it was annotated as 'NREM sleep' and the rest of the clusters were annotated as 'REM sleep'.

In manual scoring, each epoch was staged by visual inspection as NREM, REM, and Wake by the following criteria: An epoch was staged as NREM sleep when it was characterized by high-amplitude EEG waves with low-frequency (0.5–4 Hz by visual inspection) dominance and very low amplitude of EMG signal. The stage of REM sleep was assigned when an epoch was characterized by low-amplitude EEG wave with a relatively high-frequency fluctuation (6–10 Hz by visual inspection) and very low EMG power. The stage of Wake was assigned when an epoch was characterized by high amplitude EMG signal.

Transition probabilities among wakefulness, NREM sleep, and REM sleep (Figures 6C, 6F, and 6G) were calculated in a similar way to P_{SW} described in the above section (Sleep measurement with SSS). For example, the transition probability from NREM sleep to wakefulness is defined as $P_{NW} = N_{NW}/(N_{NW} + N_{NR} + N_{NN})$ where N_{mn} is defined as a number of transitions from state m to n ($m,n \subseteq$ {wakefulness, NREM sleep, REM sleep}) in the observed period. Notably, in the EEG and EMG recordings, there are theoretically eight possible transitions, however, we did not take into account the transition from wakefulness to REM sleep because the transition usually does not occur in mice.

The power spectrum density for Figures 7 and S7 was calculated for each epoch by fast Fourier transformation (FFT) with Welch's averaging method (Hayes, 1996). Briefly, each 8 s segment (800 data points as the sampling frequency was at 100 Hz) was further divided into eight overlapping sequences. The length of overlap was 50% of each sequence. Hamming window was applied onto the sequences prior to the FFT and the obtained spectrum was averaged over the eight sequences. The dirty segments were excluded from the subsequent processes (Sunagawa et al., 2013). The power spectrum of each behavioral state was calculated by averaging the power spectral densities of segments within each state over the first three days of the observation period.

Visual inspection on behaviors

Two mutant mice and two control mice used in Figure 6M were randomly selected and subjected to video recordings in parallel with EEG and EMG recordings. EEG power spectrum was produced in the FASTER method (Sunagawa et al., 2013). The EEG theta-oscillation dominant periods were extracted by calculating the ratio of EEG-theta power (6-10 Hz) to delta power (0.5-4 Hz) for each epoch (EEG data with time length of 8 s). Mean and SD of the theta/delta ratios were obtained for each 12-hour interval just before and just after the sleep-deprivation for individual mice. The timestamp of epoch was reported when its theta/delta ratio exceeded the threshold of mean + 5 SD, and the associated videos were visually inspected. The inspection covered the 30-hour period prior to and 12-hour period subsequent to the sleep-deprivation. The timestamps of transition from NREM sleep to wakefulness were extracted according to annotated stages.

Sleep deprivation with SSS

Mice were sleep deprived for 1, 2, 4, and 6 h by automated shaker (NR-40, TAITEC, Japan) in a different breeding rack from the one used for SSS recordings. The shaking speed was at around 120–130 rpm, and shaking method was alternatively switched between reciprocal and rotary every two hours. Every duration of sleep deprivation (SD) ended at ZT12. After SD, mice were returned to the SSS rack and recorded for 2 days.

Sleep deprivation with EEG and EMG recordings

Mice were implanted with EEG and EMG probes and sleep deprived for 6 h (ZT6-12) by the gentle touch of a brush.

X-gal staining and fluorescent imaging of Tet reporter mice

X-gal staining of Tet reporter mice was performed as reported previously with minor modifications (Imayoshi et al., 2006). Briefly, fresh samples of adult mice brain were sliced into 400 μm sections, fixed in 2% formaldehyde and 0.2% glutaraldehyde in PBS solution for 1 h at 4°C, rinsed twice in 0.1 M phosphate buffer (PB) (pH 7.4), 2 mM $MgCl_2$, 0.01% sodium deoxycholate, 0.02% NP-40, and stained at 37°C for 4 h in X-gal stain buffer (2 mg/mL X-gal, 2 mM $MgCl_2$, 0.01% sodium deoxycholate, 0.02% NP-40, 5 mM $K_3Fe(CN)_6$, 5 mM $K_4Fe(CN)_6$ in 0.1 M PB). Stained samples were washed twice in PBS and post-fixed with 4% PFA in PBS for 2 h at room temperature (23–25°C).

Fluorescent imaging of Tet reporter mice was performed as reported previously (Susaki et al., 2014). Each fixed brain was immersed in 10 g of CUBIC reagent-1 at 37°C with gentle shaking for 3 days, then the solution was exchanged, and the sample immersed in the same volume of fresh reagent-1 for an additional 3–4 days. The treated brain was washed with PBS several times at room temperature (23–25°C) with gentle shaking, immersed in 20% (w/v) sucrose in PBS, degassed, and immersed in reagent-2 (10 g per brain) for 3–7 days. After imaging, the sample was washed again with PBS, immersed in 20% (w/v) sucrose in PBS, and stored in O.C.T. compound at −80°C. Fluorescence images were acquired with an LSFM (Ultramicroscope, LaVision BioTec, Germany) as described in the previous report (Susaki et al., 2014).

For each brain sample of CUBIC analysis, 3D NIfTI-1 files were generated from the Z stacks acquired in the dorsal-ventral (DV) and ventral-dorsal (VD) directions, merged, and registered as described previously (Susaki et al., 2014; Susaki et al., 2015). We normalized the tdTomato signals and used the NIfTI-1 images aligned to the Allen Brain Atlas (Lein et al., 2007) to extract only pixels located inside the brain. We calculated the median intensity of these pixels for each brain and normalized the data so that all brain samples had the same median intensity.

Activated cells were detected in the image stack using Fiji software (Schindelin et al., 2012). For each horizontal slice of a given brain sample, we started by subtracting the background (rolling ball radius: 2 pixels). We then calculated a Gaussian blur (sigma: 2) and subtracted from the image in order to preserve only the signal of interest. We then successively ran the ''setThreshold'' (with parameters 800, 65536), ''Threshold,'' and ''Analyze Particles'' (with size = 2–25, circularity = 0.3–1.0) commands. The number of activated cells in a brain sample was calculated as the sum of the number of cells identified in each of its slices.

When processing each slice, we also saved an image containing only the detected activated cells in order to reconstruct 3D images of cell activation throughout the brain.

To analyze local patterns, we aligned these images to the brain atlas using the registration parameters calculated above. Analyzing aligned samples meant that we did not have access to single-cell resolution, and the Fiji-based cell detection method could not be applied. However, it was previously shown that the intensity of the extracted signal could be used to estimate the number of activated cells with $R^2 \approx 0.95$ (Tatsuki et al., 2016).

We extracted the detected signal corresponding to this specific region in the Allen Brain Atlas. To filter out noise, we focused on regions with a non-zero signal in at least 3 of the 9 brains. For these regions, hierarchical clustering was performed in R (R Development Core Team, 2016). We identified a cluster of 99 regions (out of the 1203 regions defined on the reference atlas) with no (or close to no) signal in *TrkA-tTA*(-);tetO-*tdTomato*(+) brains, and reliable signal in *TrkA-tTA*(+);tetO-*tdTomato*(+) brains. For this cluster, we generated a whole-brain mask to extract and reconstruct a 3D image of the cell signal specific to these 99 regions.

In situ hybridization

Probes against *TrkA*, *Ngfr,* and *ChAT* were amplified from mouse brain cDNA (C57BL6/N, male), and *Egfp and mNeonGreen* were amplified from plasmids by PCR. Probes against *VGluT1* (kindly provided by Dr. Kazunari Miyamichi) were amplified from mouse brain cDNA (first strand cDNA mouse brain MD01, GenoStaff). All the probe fragments were cloned into pCR-BluntII-TOPO vector (Thermo Fisher Scientific, MA, U.S.A.) for storage, and *in vitro* transcription (IVT) templates were generated by PCR using the cloned vector. All primers used for cloning and IVT reactions are listed in Table S1. Probe labeling and purification were conducted using the same protocol described in the previous paper (Tatsuki et al., 2016). Probes for *ChAT*-1 and *ChAT*-2 were mixed before hybridization.

For fluorescence *in situ* hybridization (FISH), mice were sacrificed at ZT5, and the brain was used for the same procedures described previously (Tatsuki et al., 2016).

For NBT-BCIP staining, mice were sacrificed at ZT5, and the same procedures were performed until the blocking step of the FISH protocol. After blocking, the sections were incubated with the blocking buffer containing anti-Dig-Fab-AP (Merck, Germany; #11093274910, 1:1000) overnight at 4°C. The next day, the sections were washed three times in PBS containing 0.3% Triton X-100 (PBST) for 10 min each, then incubated in NTMT solution (50 mM $MgCl_2$, 100 mM NaCl, 100 mM Tris-HCl (pH 9.5), 1% Tween-20) for 5 min, and incubated in NTMT solution containing NBT/BCIP stock solution (Merck, Germany; 1:50) for 4–5 days at 4°C. The sections were incubated in TE buffer for 5 min and embedded with 80% glycerol.

Images of *in situ* hybridization samples were acquired with a BX51 inverted confocal microscope (Olympus, Japan). A series of images covering all areas of a section were acquired and stitched with the pairwise stitching plugin of ImageJ (Preibisch et al., 2009).

QUANTIFICATION AND STATISTICAL ANALYSIS

Statistical analyses were performed by Microsoft Excel for Mac version 15.40, R version 3.1.0., Wolfram Mathematica version 9.0.1.0, 11.2.0.0.

For paired samples, the normality was tested by Shapiro test at a significance level of 0.05. When normality was not rejected in both groups, the homogeneity of variance was tested by *F*-test at a significance level of 0.05. When the null hypothesis of normal distribution with equal variance for the two groups was not rejected, a Student's paired t test was used, otherwise a two-sample Wilcoxon t test was applied.

For unpaired two samples, the means of two sets of data were evaluated. The normality was tested by the Shapiro test at a significance level of 0.05. When the normality was not rejected in both groups, the homogeneity of variance was tested by *F*-test at a significance level of 0.05. When the null hypothesis of normal distribution with equal variance for the two groups was not rejected, a Student's t test was used. When the normality was not rejected but the null hypothesis of equal variance was rejected, a Welch's t test was used. Otherwise, a two-sample Wilcoxon test was applied.

For comparing more than two samples (i.e., CRISPR mutant mice) against identical one sample (i.e., C57BL/6N control mice), data means were evaluated. The normality was tested by the Kolmogorov-Smirnov test at a significance level of 0.05. When the normality was not rejected in all groups, the homogeneity of variance was tested by Bartlett's test at a significance level of 0.05. When the null

hypothesis of normal distribution with equal variance was not rejected for all groups, Dunnett's test was used, otherwise the Steel test was applied.

In this study, $p < 0.05$ was considered significant (*$p < 0.05$, **$p < 0.01$, ***$p < 0.001$, and n.s. for not significant).

DATA AND SOFTWARE AVAILABILITY

Genome-wide mRNA expression profiles of BF/POA region analyzed along with data from 48 other brain regions which we made public at the database (http://poabf.brainstars.org/).

Cell Reports, Volume *24*

Supplemental Information

Muscarinic Acetylcholine Receptors *Chrm1* and *Chrm3* Are Essential for REM Sleep

Yasutaka Niwa, Genki N. Kanda, Rikuhiro G. Yamada, Shoi Shi, Genshiro A. Sunagawa, Maki Ukai-Tadenuma, Hiroshi Fujishima, Naomi Matsumoto, Koh-hei Masumoto, Mamoru Nagano, Takeya Kasukawa, James Galloway, Dimitri Perrin, Yasufumi Shigeyoshi, Hideki Ukai, Hiroshi Kiyonari, Kenta Sumiyama, and Hiroki R. Ueda

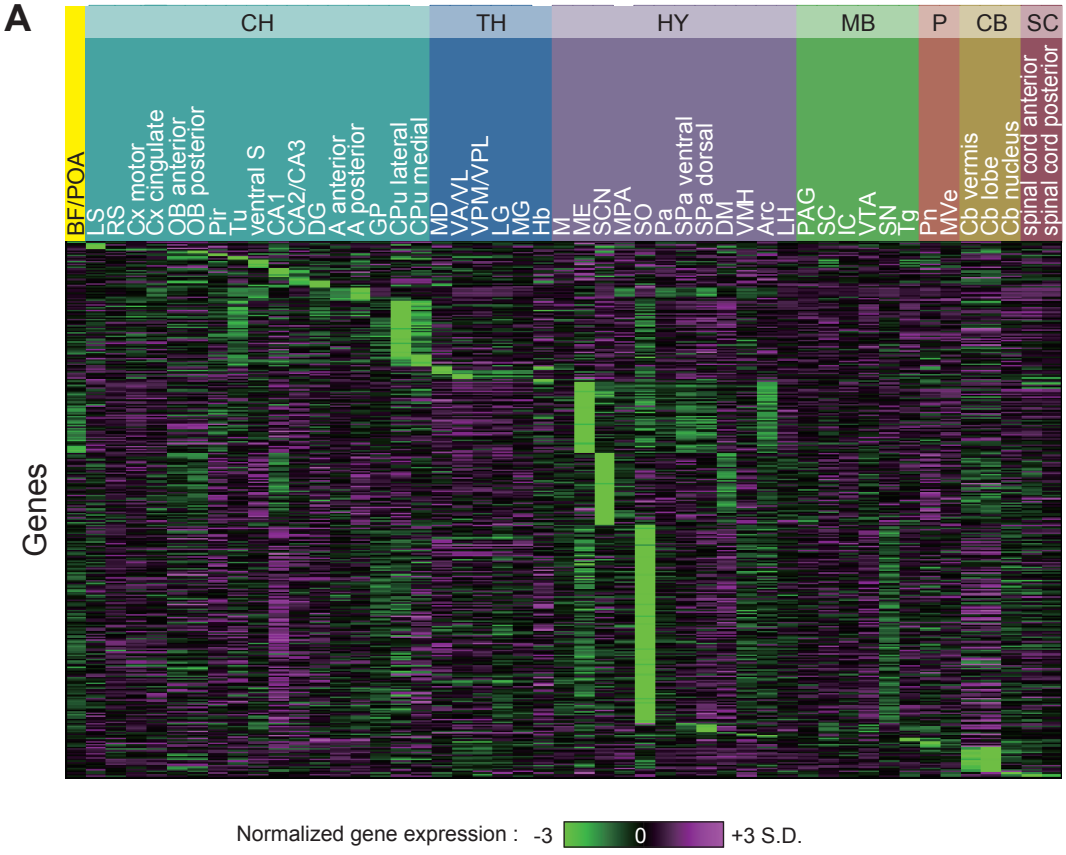
A
CH
TH
HY
MB
P
CB
SC
BF/POA
LS
RS
Cx motor
Cx cingulate
OB anterior
OB posterior
Pir
Tu
ventral S
CA1
CA2/CA3
DG
A anterior
A posterior
GP
CPu lateral
CPu medial
MD
VA/VL
VPM/VPL
LG
MG
Hb
M
ME
SCN
MPA
SO
Pa
SPa ventral
SPa dorsal
DM
VMH
Arc
LH
PAG
SC
IC
VTA
SN
Tg
Pn
MVe
Cb vermis
Cb lobe
Cb nucleus
spinal cord anterior
spinal cord posterior
Genes
Normalized gene expression : -3 0 +3 S.D.

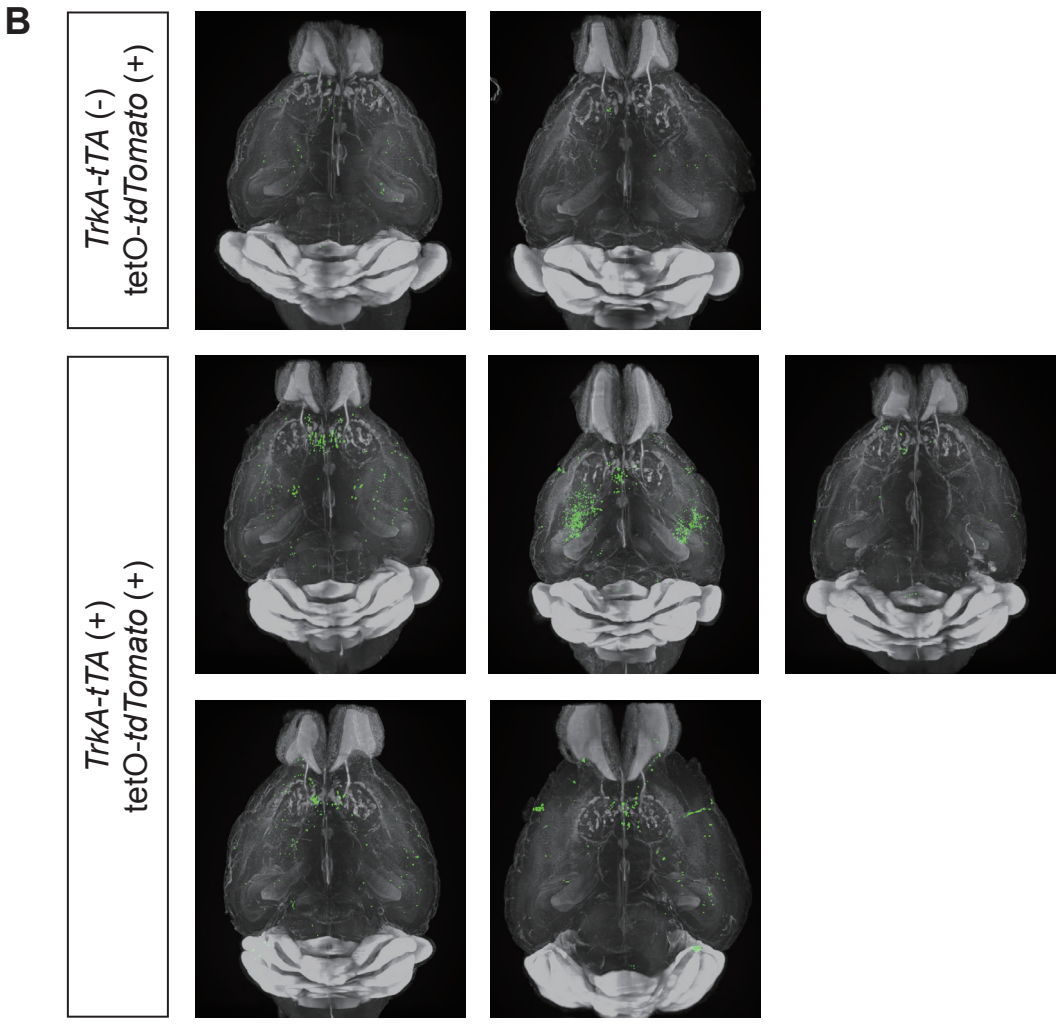
B
TrkA-tTA (-)
tetO-tdTomato (+)
TrkA-tTA (+)
tetO-tdTomato (+)

Figure S1. Identification of marker genes in the BF/POA region and establishment of *TrkA-tTA* mice. Related to Figure 1

A, The mRNA expression profiles in 49 distinct brain regions are represented in a heatmap. Genes whose expression was decreased in one of those regions were selected from the genome-wide dataset. Each row corresponds to a gene, and each column to a region designated at the top of the panel. CH, cerebrum. TH, thalamus. HY, hypothalamus. MB, midbrain. P, pons. CB, cerebellum. SC, spinal cord. BF/POA, basal forebrain/preoptic area. LS, lateral septal nucleus. RS, retrosplenial cortex. Cx motor, cerebral cortex motor. Cx cingulate, cerebral cortex cingulate. OB anterior, olfactory bulb anterior. OB posterior, olfactory bulb posterior. Pir, piriform cortex. Tu, olfactory tubercle. ventral S, ventral subiculum. CA1, CA1 (hippocampus). CA2/CA3, CA2/CA3 (hippocampus). DG, dentate gyrus (hippocampus). A anterior, amygdala anterior. A posterior, amygdala posterior. GP, globus pallidus. CPu lateral, caudate putamen lateral. CPu medial, caudate putamen medial. MD, mediodorsal thalamic nucleus. VA/VL, ventral anterior thalamic nucleus/ventrolateral thalamic nucleus. VP/VPL, ventral posteromedial thalamic nucleus/ventral posterolateral thalamic nucleus. LG, lateral geniculate body. MG, medial geniculate nucleus. Hb, habenular nucleus. Pineal, corpus pineal. M, mammillary body. ME, median eminence. SCN, suprachiasmatic nucleus. MPA, medial preoptic area. SO, supraoptic nucleus. Pa, paraventricular hypothalamic nucleus. SPa ventral, subparaventricular zone ventral. SPa dorsal, subparaventricular zone dorsal. DM, dorsomedial hypothalamic nucleus. VMH, ventromedial hypothalamic nucleus. Arc, arcuate hypothalamic nucleus. LH, lateral hypothalamus. PAG, periaqueductal gray. SC, superior colliculus. IC, inferior colliculus. VTA, ventral tegmental area. SN, substantia nigra. Tg, dorsal tegmental nucleus. Pn, pontine nucleus. MVe, medial vestibular nucleus. Cb vermis, cerebellar cortex vermis. Cb lobe, cerebellar cortex lobe. Cb nucleus, cerebellar nucleus. **B,** The expression of a reporter gene driven by *TrkA-tTA* in the BF/POA region of the brain. Brains of mice harboring tetO-*tdTomato* transgene with and without *TrkA-tTA* transgene were imaged and analyzed as in **Figure 1I**. The tdTomato signal is shown in the reconstituted 3D image for brains of tetO-*tdTomato(+);TrkA-tTA(-)* (top row) and brains of tetO-*tdTomato(+);TrkA-tTA(+)* (lower two rows). All analyzed brains are presented except the representative ones shown in **Figure 1I**. Gray dots represent nuclear signal of RedDot2; green dots represent cells in the 99 detected regions. Scale bar, 2 mm.

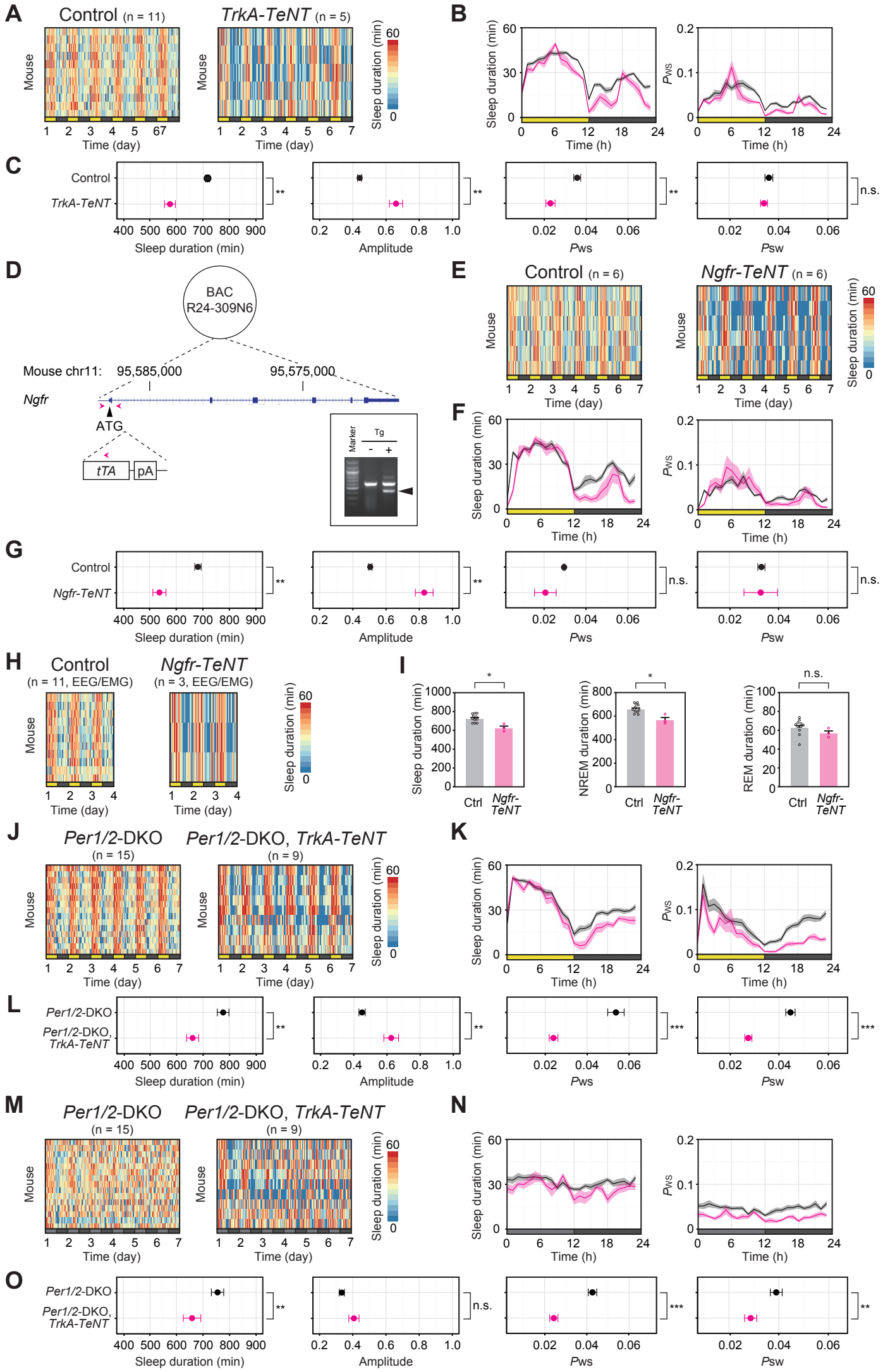

Niwa et al. Figure S2

Figure S2. Sleep phenotype of *TrkA-TeNT* mice in the no-dox condition and in the *Per1*, *Per2* DKO background and that of *Ngfr-TeNT* mice. Related to Figure 2

A-C, Sleep phenotype of *TrkA-TeNT* mice (n = 5) and control littermates (n = 11) maintained in the no-dox condition measured by SSS. **A,** Heatmap representation of sleep duration (per hour) over 6 days. **B,** Sleep duration and P_{WS} (per hour) over 24 h averaged over 6 days. The mean at each hour of the day is plotted for *TrkA-TeNT* mice (magenta line), and for control littermates (black line). Shaded area around line represents standard error of mean (SEM). **C,** Sleep/wake parameters. Sleep duration is the total sleep duration in a day, amplitude is related to the variation of sleep duration (per hour) within the daily sleep cycle, P_{WS} and P_{SW} are the respective transition probabilities from wakefulness to sleep and vice versa. **D,** Schematic representation of modified BAC where tTA and polyA signal were inserted just after the start codon of the *Ngfr* gene and PCR confirmation for genotypes of established BAC transgenic mice (inset). **E-G,** Sleep phenotype of *Ngfr-TeNT* mice (n = 6) and control littermates (n = 6) maintained in the no-dox condition measured by SSS. **E,** Heatmap representation of sleep duration (per hour) over 6 days. **F,** Sleep duration and P_{WS} (per hour) over 24 h averaged over 6 days. The mean at each hour of the day is plotted for *Ngfr-TeNT* mice (magenta line) and for control mice (black line). Shaded area represents SEM. **G,** Sleep/wake parameters are presented as in (**c**). **H, I,** Sleep phenotype of *Ngfr-TeNT* mice (n = 3) and control littermates (n = 11) measured by EEG and EMG recordings. **H,** Heatmap representation of sleep duration (per hour) over 3 days. **I,** The duration of total sleep, NREM sleep, and REM sleep in a day. **J-O,** Sleep phenotype of *TrkA-TeNT*, *Per1/2* double KO (DKO) mice (n = 9) and control *Per1/2* DKO mice (n = 15) under LD (**J-L**) and DD (**M-O**) conditions measured by SSS. Mice were maintained with dox after birth and released from dox 4 weeks before SSS measurement. **J, M,** Heatmap representation of sleep duration (per hour) over 6 days. **K, N,** Sleep duration and P_{WS} (per hour) over 24 h averaged over 6 days. The mean at each hour of the day is plotted for *TrkA-TeNT*, *Per1/2* DKO mice (magenta line) and for control *Per1/2* DKO mice (black line). Shaded area represents SEM. **L, O,** Sleep/wake parameters. Sleep duration is the total sleep duration in a day, amplitude is related to the variation of sleep duration (per hour) within the daily sleep cycle, P_{WS} and P_{SW} are the respective transition probabilities from wakefulness to sleep and vice versa. Error bars, SEM. $*P < 0.05$, $**P < 0.01$, $***P < 0.001$.

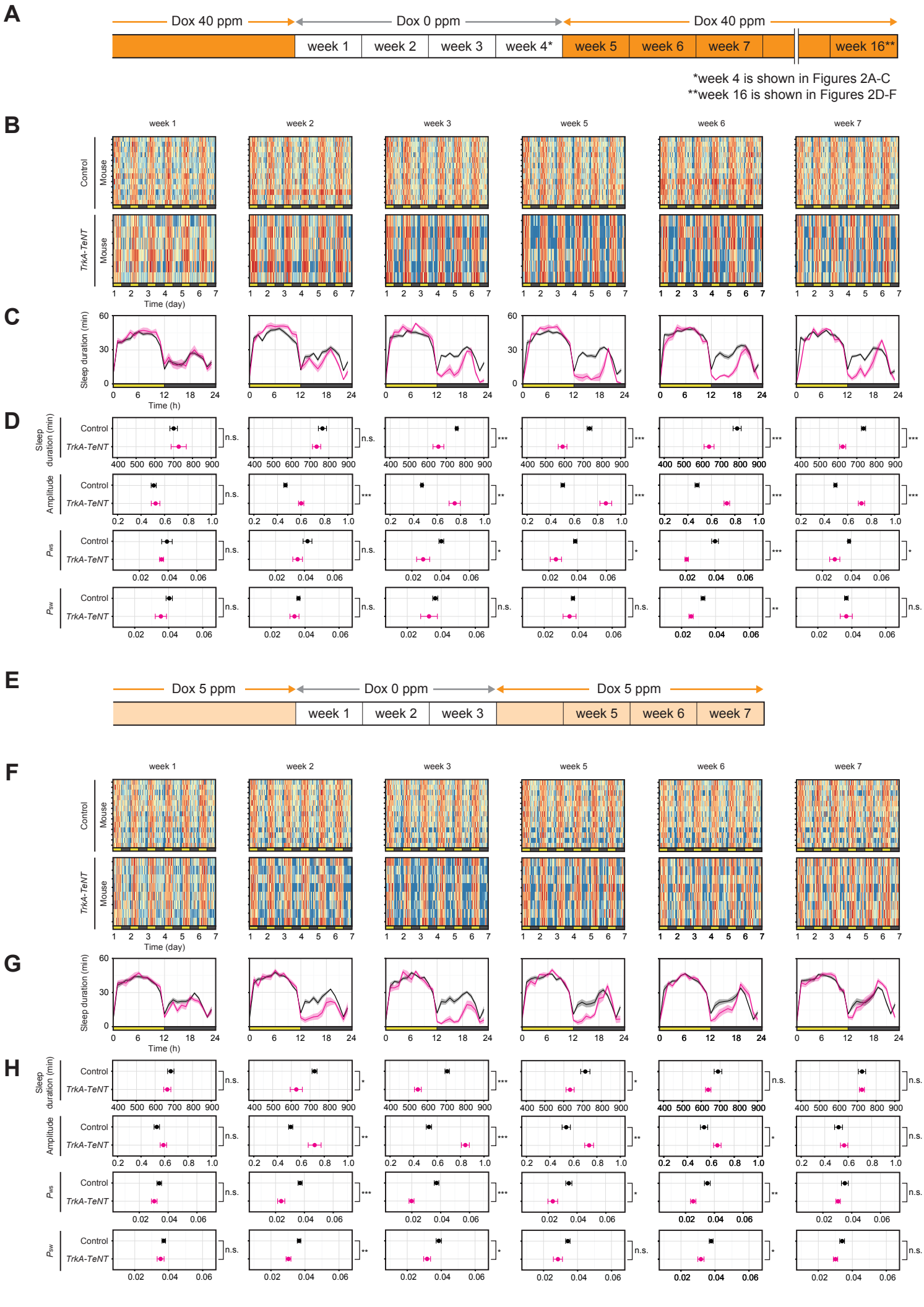

Niwa et al. Figure S3

Figure S3. Sleep phenotype of *TrkA-TeNT* mice in the 40 ppm and 5 ppm dox-on and dox-off conditions. Related to Figure 2

A, Experimental protocol of 40 ppm doxycycline (dox) treatment of *TrkA-TeNT* mice and control littermates (also shown in **Figure S4A**). The data of week 4 and week 16 are shown in **Figure 2A-C** and **D-F**, respectively. **B-D**, Sleep phenotype of *TrkA-TeNT* mice (n = 6) and control littermates (n = 13) with 40 ppm dox-food measured by SSS. **B,** Heatmap representation of sleep duration (per hour) over 6 days. **C,** Sleep duration (per hour) over 24 h averaged over 6 days. The mean sleep duration at each hour of the day is plotted for *TrkA-TeNT* mice (magenta line) and for control mice (black line). Shaded area represents SEM. **D,** Sleep/wake parameters. Sleep duration is the total sleep duration in a day, amplitude is related to the variation of sleep duration (per hour) within the daily sleep cycle, P_{WS} and P_{SW} are the respective transition probabilities from wakefulness to sleep and vice versa. **E,** Experimental protocol of 5 ppm doxycycline (dox) treatment of *TrkA-TeNT* mice and control mice. **F-H,** Sleep phenotype of *TrkA-TeNT* mice (n = 8) and control littermates (n = 13) with 5 ppm dox-food measured by SSS. **F,** Heatmap representation of sleep duration (per hour) over 6 days. **G,** Sleep duration (per hour) over 24 h averaged over 6 days. The mean sleep duration at each hour of the day is plotted for *TrkA-TeNT* mice (magenta line) and for control mice (black line). Shaded area represents SEM. **H,** Sleep/wake parameters are presented as in (**D**). Error bars, SEM. $*P < 0.05$, $**P < 0.01$, $***P < 0.001$.

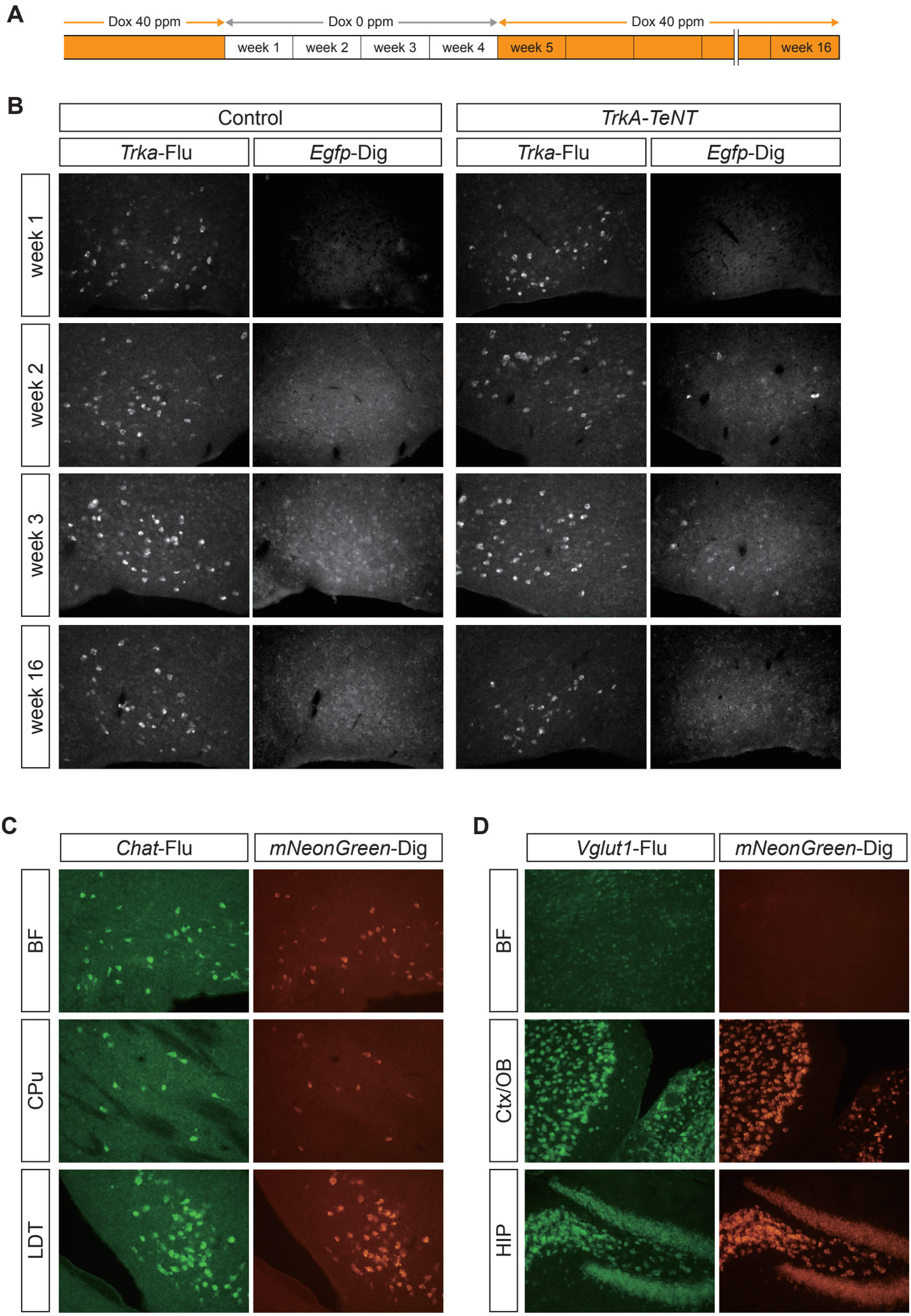

Niwa et al. Figure S4

Figure S4. Characterization of *TrkA-TeNT*, *ChAT-tTR-mNG* KI and *VGluT1-tTR-mNG* KI mice by FISH analysis. Related to Figure 2 and 3

A, Experimental protocol of doxycycline (dox) treatment on *TrkA-TeNT* mice and control littermates. Mice were maintained with dox shortly after birth. After weaning and maturation, mice were released to food without doxycycline (normal-food) and maintained for four weeks (from week 1 to week 4). On and after week 5, mice were returned to dox-food. **B,** *TeNT* expression in the BF of *TrkA-TeNT* mice and control littermates measured by fluorescent *in situ* hybridization (FISH) analysis with a fluorescein labeled *Trka* antisense RNA probe (*Trka*-Flu; green) and digoxigenin labeled *Egfp* RNA probe (*Egfp*-Dig; red) in the dox-off (week 1, week 2, week 3) and dox-on (week 16) condition. Two representative samples are shown. **C,** Colocalization of *Chat* mRNA expression (fluorescein labeled, Flu; green) and *tTR* mRNA expression (digoxigenin labeled, Dig; red) detected by antisense RNA probe for *mNeonGreen* (*mNG*) in the BF, CPu, and LDT of *ChAT-tTR-mNG* KI mice. **D,** Colocalization of *Vglut1* mRNA expression (fluorescein labeled, Flu; green) and *tTR* mRNA expression (digoxigenin labeled, Dig; red) detected by an antisense RNA probe for *mNG* in the Ctx/OB and HIP of *VGluT1-tTR-mNG* KI mice. Neither *VGluT1* nor *tTR* expression were observed in the BF. BF, basal forebrain. CPu, caudate putamen. LDT, laterodorsal tegmentum. Ctx/OB, cerebral cortex/olfactory bulb. HIP, hippocampus.

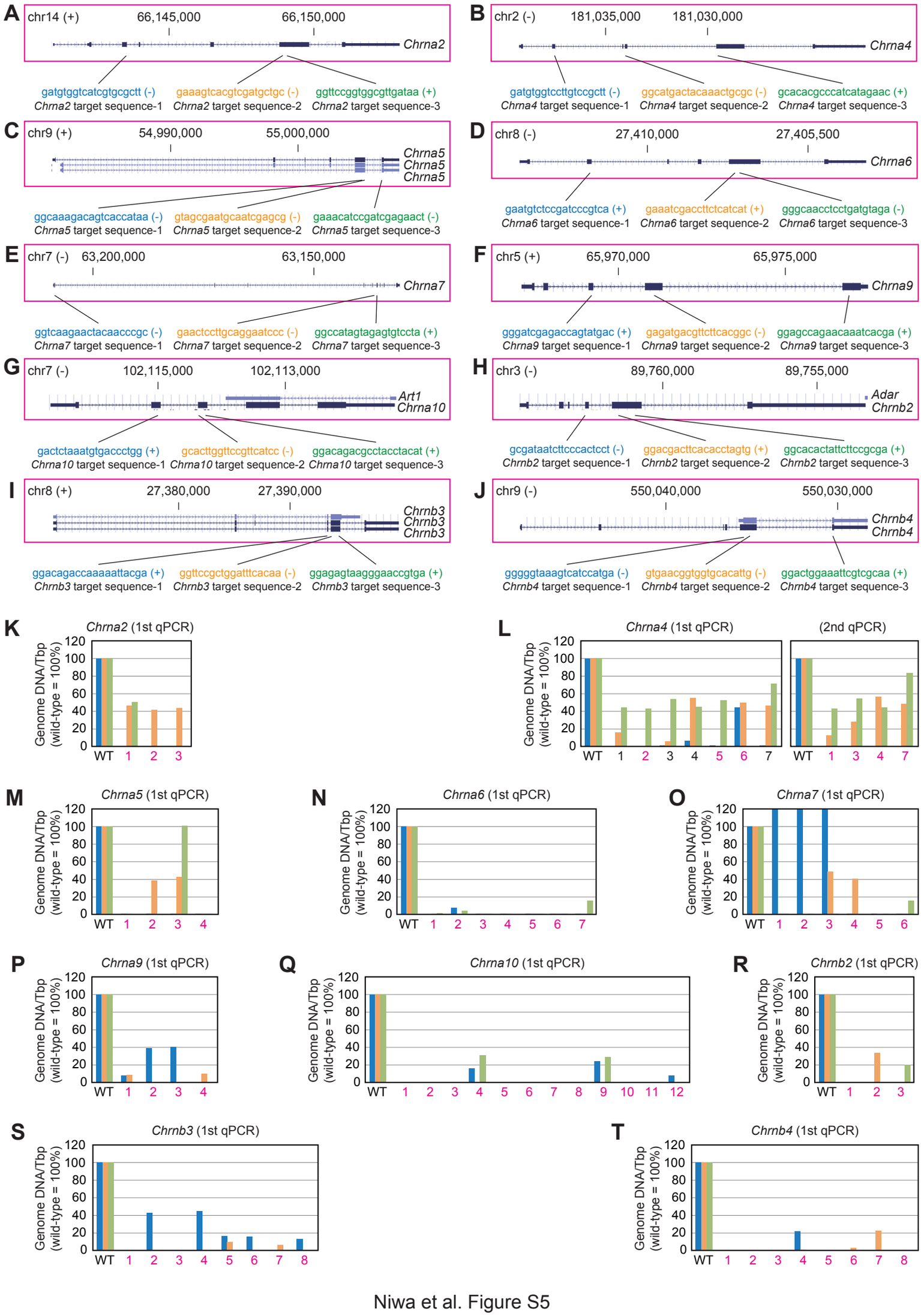

Niwa et al. Figure S5

Figure S5. Confirmation of knockout of nicotinic acetylcholine receptors. Related to Figure 4

A-J, Target sequences of the gRNAs for knockout of the nicotinic acetylcholine receptor family. *Chrna2* (**A**), *Chrna4* (**B**), *Chrna5* (**C**), *Chrna6* (**D**), *Chrna7* (**E**), *Chrna9* (**F**), *Chrna10* (**G**), *Chrnb2* (**H**), *Chrnb3* (**I**), and *Chrnb4* (**J**); each gene had three target sequences. The mouse genomic sequence data were obtained from GRCm38/mm10 via the UCSC Genome Browser (http://genome.ucsc.edu/) (Rhead et al., 2010). The colored letters (blue, orange, and green) show the 20-base target sequences. The target sequences were designed on the sense (+) or antisense (-) strand of the genomic DNA. **K-T,** The genotype of nicotinic acetylcholine receptor family KO mice. *Chrna2* (**K**), *Chrna4* (**L**), *Chrna5* (**M**), *Chrna6* (**N**), *Chrna7* (**O**), *Chrna9* (**P**), *Chrna10* (**Q**), *Chrnb2* (**R**), *Chrnb3* (**S**), and *Chrnb4* (**T**); each gene had three targets for quantitative PCR (qPCR) genotyping. The amount of intact DNA for each target sequence was measured by qPCR. The genomic DNA was purified from tail of each mouse. The amount of measured DNA of KO mice for each target sequence is expressed as the percentage of that of wild-type mouse. Number and WT below the bar plot denote the ID of KO mouse and the wild-type mouse, respectively. KO mice, which were confirmed by the relative DNA amount of less than 0.5% by at least one of three targets, are labelled in magenta otherwise in black. *TATA-binding protein* (*Tbp*) was used as internal control. Color of bars correspond to that of gRNA sequences.

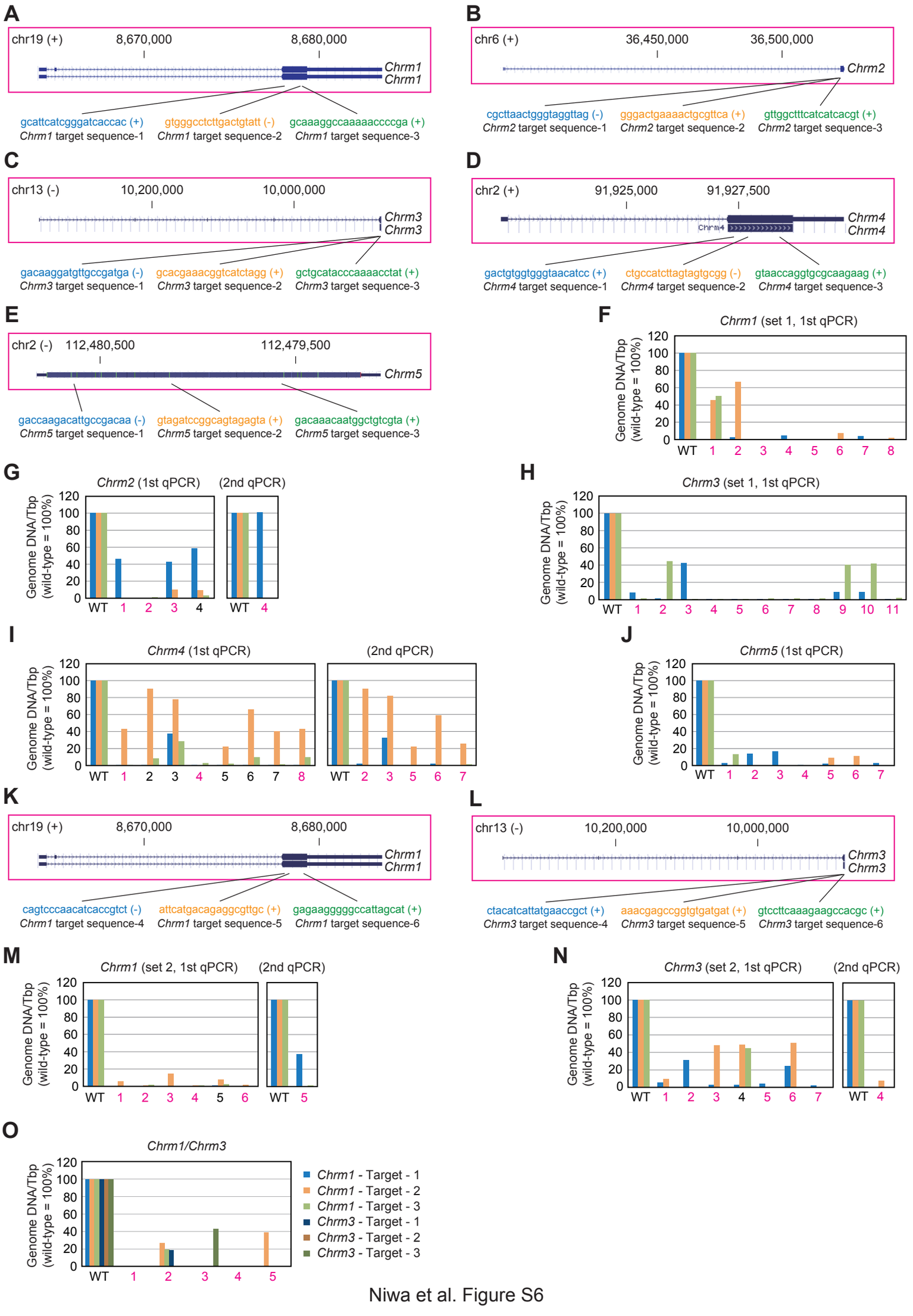

Niwa et al. Figure S6

Figure S6. Confirmation of knockout of muscarinic acetylcholine receptors. Related to Figure 5, 6 and 7

A-E, K, L, Target sequences of the gRNAs for knockout of the muscarinic acetylcholine receptor family. *Chrm1* (set 1, **A**), *Chrm2* (**B**), *Chrm3* (set 1, **C**), *Chrm4* (**D**), *Chrm5* (**E**), *Chrm1* (set 2, **K**), and *Chrm3* (set 2, **L**); each gene had three target sequences. The mouse genomic sequence data were obtained from GRCm38/mm10 via the UCSC Genome Browser (http://genome.ucsc.edu/) (Rhead et al., 2010). The colored letters (blue, orange, and green) show the 20-base target sequences. The target sequences were designed on the sense (+) or antisense (-) strand of the genomic DNA. **F-J, M-O,** The genotype of muscarinic acetylcholine receptor family KO mice. *Chrm1* (set 1, **F**), *Chrm2* (**G**), *Chrm3* (set 1, **H**), *Chrm4* (**I**), *Chrm5* (**J**), *Chrm1* (set 2, **M**), *Chrm3* (set 2, **N**), and *Chrm1*/*3* (**O**); each gene had three targets for quantitative PCR (qPCR) genotyping. The amount of intact DNA for each target sequence was measured by qPCR. The genomic DNA was purified from tail of each mouse. The amount of measured DNA of KO mice for each target sequence is expressed as the percentage of that of wild-type mouse. Number and WT below the bar plot denote the ID of KO mouse and the wild-type mouse, respectively. KO mice, which were confirmed by the relative DNA amount of less than 0.5% by at least one of three targets, are labelled in magenta otherwise in black. *TATA-binding protein* (*Tbp*) was used as internal control. Color of bars correspond to that of gRNA sequences.

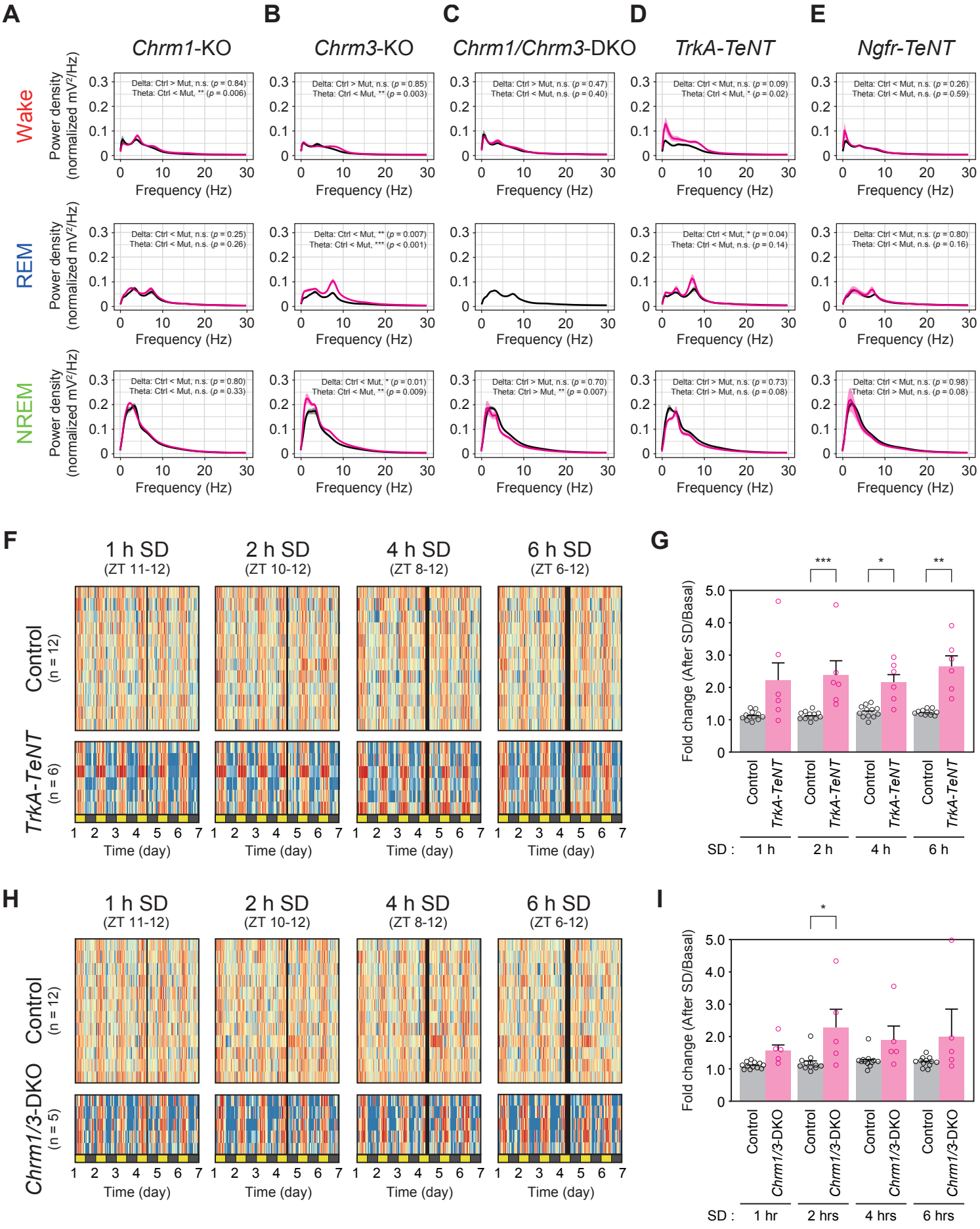
A
B
C
D
E
Chrm1-KO
Chrm3-KO
Chrm1/Chrm3-DKO
TrkA-TeNT
Ngfr-TeNT
Wake
REM
NREM
Power density (normalized mV²/Hz)
Frequency (Hz)
Delta: Ctrl > Mut, n.s. (p = 0.84)
Theta: Ctrl < Mut, ** (p = 0.006)
Delta: Ctrl > Mut, n.s. (p = 0.85)
Theta: Ctrl < Mut, ** (p = 0.003)
Delta: Ctrl > Mut, n.s. (p = 0.47)
Theta: Ctrl < Mut, n.s. (p = 0.40)
Delta: Ctrl < Mut, n.s. (p = 0.09)
Theta: Ctrl < Mut, * (p = 0.02)
Delta: Ctrl < Mut, n.s. (p = 0.26)
Theta: Ctrl < Mut, n.s. (p = 0.59)
Delta: Ctrl < Mut, n.s. (p = 0.25)
Theta: Ctrl < Mut, n.s. (p = 0.26)
Delta: Ctrl < Mut, ** (p = 0.007)
Theta: Ctrl < Mut, *** (p < 0.001)
Delta: Ctrl < Mut, * (p = 0.04)
Theta: Ctrl < Mut, n.s. (p = 0.14)
Delta: Ctrl < Mut, n.s. (p = 0.80)
Theta: Ctrl < Mut, n.s. (p = 0.16)
Delta: Ctrl < Mut, n.s. (p = 0.80)
Theta: Ctrl < Mut, n.s. (p = 0.33)
Delta: Ctrl < Mut, * (p = 0.01)
Theta: Ctrl < Mut, ** (p = 0.009)
Delta: Ctrl > Mut, n.s. (p = 0.70)
Theta: Ctrl > Mut, ** (p = 0.007)
Delta: Ctrl > Mut, n.s. (p = 0.73)
Theta: Ctrl > Mut, n.s. (p = 0.08)
Delta: Ctrl < Mut, n.s. (p = 0.98)
Theta: Ctrl > Mut, n.s. (p = 0.08)
F
1 h SD (ZT 11-12)
2 h SD (ZT 10-12)
4 h SD (ZT 8-12)
6 h SD (ZT 6-12)
Control (n = 12)
TrkA-TeNT (n = 6)
Time (day)
G
Fold change (After SD/Basal)
***
*
**
Control
TrkA-TeNT
SD : 1 h 2 h 4 h 6 h
H
1 h SD (ZT 11-12)
2 h SD (ZT 10-12)
4 h SD (ZT 8-12)
6 h SD (ZT 6-12)
Control (n = 12)
Chrm1/3-DKO (n = 5)
Time (day)
I
Fold change (After SD/Basal)
*
Control
Chrm1/3-DKO
SD : 1 hr 2 hrs 4 hrs 6 hrs

Figure S7. FFT power spectrum on EEG/EMG recording and the response of *TrkA-TeNT* and *Chrm1/3*-DKO mice to sleep-deprivation. Related to Figure 2, 6 and 7

A-E, FFT frequency spectrum of *Chrm1* KO (**A**), *Chrm3* KO (**B**), *Chrm1/Chrm3* DKO (**C**), *TrkA-TeNT* (**D**), and *Ngfr-TeNT* (**E**) mice. The mean power density at each frequency is plotted for mutant mice (magenta line) and for control mice (black line). All the time series of EEG data were normalized so that the standard deviation of the first 24 hours becomes 1 before calculating the power spectrum. Shaded area represents SEM. Statistical results are shown in inset. **F-I**, The duration of sleep measured by SSS before and after sleep-deprivation (SD). SD was applied for durations of 1, 2, 4, and 6 h by automated shaker. SD of each duration ended at ZT12. **F, G,** The phenotypes of sleep-deprived *TrkA-TeNT* mice (n = 6) and control littermates (n = 12). **H, I,** The phenotypes of sleep-deprived *Chrm1/3* double KO (DKO) mice (n = 5) and control C57BL/6N mice, used in **Figure 6H-J**. **F, H,** Heatmap representation of sleep duration (per hour) measured by SSS over 6 days. **G, I,** Fold change of sleep duration induced by SD. Each sleep duration of "After SD" and "Basal" respectively corresponds to the sleep duration of ZT12–24 subsequent to SD and the averaged sleep duration of ZT12-24 in three days before the day of SD. Error bars, SEM. $*P < 0.05$, $**P < 0.01$, $***P < 0.001$.

SUPPLEMENTAL TABLES

Table S1. Primers for RNA probes of *in situ* hybridization in this study. Related to Figure 1 and 3

Anti-sense RNA probes for *TrkA*, *Ngfr*, *Egfp*, *mNeonGreen*, *ChAT*, and *VGluT1* were produced by *in vitro* transcription with T3-probe PCR fragments. *ChAT* probes were used as mixes of *ChAT-1* and *2*. T3 promoter sequence is underlined.

Gene	Primer	Sequence
Trka	Forward	5'-cctactgagggcaaaggctccggact-3'
	Reverse	5'-aattaaccctcactaaaggggtagacatcaggagggcaggcg-3'
Ngfr	Forward	5'-tacgttctctgacgtggtaagc-3'
	Reverse	5'-aattaaccctcactaaagggagtctatatgctccggctggta-3'
Egfp	Forward	5'-cccatcctggtcgagctggacg-3'
	Reverse	5'-aattaaccctcactaaagggcacgaactccagcaggaccatg-3'
mNeonGreen	Forward	5'-taacatggcctctctcccagcg-3'
	Reverse	5'-aattaaccctcactaaagggcacatcggtaaaggccttttgc-3'
Chat (Probe #1)	Forward	5'-ccccccaaagatgcctgtacaagc-3'
	Reverse	5'-aattaaccctcactaaagggcctggaccatccaggcataccag-3'
Chat (Probe #2)	Forward	5'-ggtggaggctgcagcttgaatgga-3'
	Reverse	5'-aattaaccctcactaaagggcaggctccatacccattgggtacc-3'
Vglut1 (*Slc17a7*)	Forward	5'-ctggcagtgacgaaagtgaa-3'
	Reverse	5'-aattaaccctcactaaagggacacaacaaatggccactga-3'